Development/Plasticity/Repair

Akt Regulates Sox10 Expression to Control Oligodendrocyte Differentiation via Phosphorylating FoxO1

He Wang,[1] Mengjia Liu,[1] ⬤Zhuoyang Ye,[1] Cuihua Zhou,[2] Huiru Bi,[1] Long Wang,[1] ⬤Chen Zhang,[3] Hui Fu,[4] ⬤Ying Shen,[5] Jian-Jun Yang,[6] Yimin Hu,[2] and ⬤Guiquan Chen[1]

[1]Ministry of Education (MOE) Key Laboratory of Model Animal for Disease Study, Model Animal Research Center, Jiangsu Key Laboratory of Molecular Medicine, Medical School, Nanjing University, Nanjing 210061, People's Republic of China, [2]Department of Anesthesiology, The Second Affiliated Changzhou People's Hospital of Nanjing Medical University, Changzhou 213000, People's Republic of China, [3]School of Basic Medical Sciences, Beijing Key Laboratory of Neural Regeneration and Repair, Advanced Innovation Center for Human Brain Protection, Capital Medical University, Beijing 100069, People's Republic of China, [4]School of Basic Medical Sciences, Wuhan University, Wuhan 430071, People's Republic of China, [5]Department of Neurobiology, Key Laboratory of Medical Neurobiology of the Ministry of Health, Zhejiang University School of Medicine, Hangzhou 310058, People's Republic of China, and [6]Department of Anesthesiology, Pain and Perioperative Medicine, The First Affiliated Hospital of Zhengzhou University, Zhengzhou 450052, People's Republic of China

Sox10 is a well known factor to control oligodendrocyte (OL) differentiation, and its expression is regulated by Olig2. As an important protein kinase, Akt has been implicated in diseases with white matter abnormalities. To study whether and how Akt may regulate OL development, we generated OL lineage cell-specific *Akt1/Akt2/Akt3* triple conditional knock-out (*Akt* cTKO) mice. Both male and female mice were used. These mutants exhibit a complete loss of mature OLs and unchanged apoptotic cell death in the CNS. We show that the deletion of Akt three isoforms causes downregulation of Sox10 and decreased levels of phosphorylated FoxO1 in the brain. *In vitro* analysis reveals that the expression of FoxO1 with mutations on phosphorylation sites for Akt significantly represses the *Sox10* promoter activity, suggesting that phosphorylation of FoxO1 by Akt is important for Sox10 expression. We further demonstrate that mutant FoxO1 without Akt phosphorylation epitopes is enriched in the Sox10 promoter. Together, this study identifies a novel FoxO1 phosphorylation-dependent mechanism for Sox10 expression and OL differentiation.

Key words: Akt; FoxO1; myelination; oligodendrocyte differentiation; Sox10

Significance Statement

Dysfunction of Akt is associated with white matter diseases including the agenesis of the corpus callosum. However, it remains unknown whether Akt plays an important role in oligodendrocyte differentiation. To address this question, we generated oligodendrocyte lineage cell-specific *Akt1/Akt2/Akt3* triple-conditional knock-out mice. Akt mutants exhibit deficient white matter development, loss of mature oligodendrocytes, absence of myelination, and unchanged apoptotic cell death in the CNS. We demonstrate that deletion of Akt three isoforms leads to downregulation of Sox10, and that phosphorylation of FoxO1 by Akt is critical for Sox10 expression. Together, these findings reveal a novel mechanism to regulate Sox10 expression. This study may provide insights into molecular mechanisms for neurodevelopmental diseases caused by dysfunction of protein kinases.

Introduction

Akt is a serine/threonine (Ser/Thr) kinase and belongs to the AGC family of protein kinases (Pearce et al., 2010). It is well known that Akt plays important roles in cell growth, cell survival, metabolism, and human diseases (Fruman et al., 2017; Manning and Toker, 2017). Akt consists of Akt1, Akt2, and Akt3, and these isoforms are highly expressed in the mammalian CNS (Easton et al., 2005; Manning and Cantley, 2007; Wang et al., 2015). However, each isoform contributes to a certain proportion of the total Akt activity. For example, Akt1, Akt2, and Akt3 account for ~30%, 20%, and 50% of the total Akt in the adult

mouse brain, respectively (Easton et al., 2005). Abundant evidence has shown that Akt isoforms play differential roles in different physiological processes including development, cell metabolism, cell size, synaptic plasticity, and spatial learning (Dummler and Hemmings, 2007; Levenga et al., 2017; Wang et al., 2017; Zhang et al., 2019).

The mammalian CNS consists of the white matter (WM) and the gray matter (GM). Oligodendrocyte (OL) is a major type of glia in the WM, and its function is to produce myelin. During the myelination process, numerous myelin proteins are expressed in premyelinating OLs, and the myelin sheath is then formed to wrap up axons. Myelin is essential for saltatory conduction of action potentials. The database in the Allen Atlas (http://mouse.brain-map.org) provides evidence showing that Akt1, Akt2, and Akt3 are expressed in WM subregions including the corpus callosum (CC) in adult mice. The following studies suggest that Akt is critical for myelination. First, it was demonstrated that the deletion of Akt3 causes reduced thickness of the CC (Tschopp et al., 2005). Second, overexpression of a constitutively active Akt induces enhanced myelination but does not affect OL population in the CNS (Flores et al., 2008). Third, it has been shown that the inhibition of Akt in dorsal root ganglion neuron–Schwann cell cocultures decreases myelin sheath formation, and that the expression of activated Akt in Schwann cells increases expression of myelin proteins (Domènech-Estévez et al., 2016). Fourth, we recently reported that the deletion of Akt3 leads to decreased expression of myelin basic protein (Mbp) and myelin-associated glycoprotein (Mag) in the CNS (Wang et al., 2017). However, it is not well understood whether Akt is important for OL differentiation in the CNS.

OL development involves several important processes (Rowitch and Kriegstein, 2010; Mayoral and Chan, 2016). First, neural progenitor cells generate OL precursor cells (OPCs). Second, OPCs proliferate and migrate throughout the whole CNS (Mayoral and Chan, 2016). Third, whereas some OPCs give rise to OLs in their final position, the others retain their stemness in their whole life (Nishiyama et al., 2012). It is well known that transcriptional factor (TF) Sox10 plays a pivotal role in OL differentiation (Elbaz and Popko, 2019). It has recently been demonstrated that Sox10 expression is regulated by Olig2 through a conserved enhancer in Sox10 (Werner et al., 2007; Küspert et al., 2011). However, it remains unknown whether Akt may regulate Sox10 expression.

Whereas accumulating evidence has shown that Akt is implicated in the 1q43-q44 microdeletion syndrome, a disease with WM abnormalities and agenesis of the CC (Boland et al., 2007; Ballif et al., 2012; Gai et al., 2015), the underlying mechanisms are poorly understood. To overcome the embryonic lethality problem caused by straight deletion of the three Akt isoforms (Dummler and Hemmings, 2007; Wang et al., 2015), we generated OL lineage cell-specific Akt triple-conditional KO (Akt cTKO) mice to study the role of Akt in OPC/OL development. We show that the loss of total Akt causes a complete absence of OL differentiation in the CNS. We report that the expression of a mutant FoxO1 without Akt phosphorylation sites significantly represses the promoter activity of Sox10. We demonstrate that mutant FoxO1 is enriched in the Sox10 promoter. Overall, this study uncovers an essential role of Akt in WM development and identifies a novel phosphorylation-dependent mechanism to regulate Sox10 expression and OL differentiation in the CNS.

Materials and Methods

Generation of floxed Akt3 mice. In the gene-targeting strategy, a neomycin (NEO) resistance cassette was flanked by two flippase recognition target (FRT) (open triangle) and one locus of X-over in P1 (loxP) element (solid triangle) sites. Another loxP with a BamHI site was introduced into intron 2 to allow conditional removal of exon 3. A herpes simplex virus-thymidine kinase (HSV-TK) was included in the targeting vector for negative selection. R1 embryonic stem (ES) cells were electroporated with the targeting vector. Southern blotting confirmed properly recombined ES cells. Homologously recombined clones were injected into blastocysts of C57BL/6 mice to generate chimeric mice. The latter were crossed to B6 mice to obtain $Akt3^{fln/+}$, which were crossed to a flippase deleter (flper) mouse (Cheng et al., 2019) to remove the NEO cassette.

Animals. $Akt1^{f/f}$, $Akt1^{-/-}$, $Akt2^{-/-}$, and $Akt3^{-/-}$ mice were reported by us previously (Wang et al., 2015, 2017). We generated Akt cTKO mice ($Akt1^{f/f};Akt2^{-/-};Akt3^{f/f};Olig1$-Cre) through multiple breeding steps. The Olig1-Cre mouse was reported previously (Lu et al., 2002; Zhu et al., 2014; He et al., 2016). For the fluorescence-activated cell sorting (FACS) study, $Akt1^{f/f};Akt2^{-/-};Akt3^{f/f}$ animals were crossed with the mTmG mouse (Muzumdar et al., 2007) to obtain the $Akt1^{f/f};Akt2^{-/-};Akt3^{f/f};$ mTmG mouse, which was bred with $Akt1^{f/+};Akt2^{+/-};Akt3^{f/+};Olig1$-Cre to obtain $Akt1^{f/f};Akt2^{-/-};Akt3^{f/f};$ Olig1-Cre;mTmG. Since there was no significant difference in the number of $CC1^+$ or $Pdgfr\alpha^+$ cells between $Akt1^{f/+};Akt2^{+/-};Akt3^{f/+};Olig1$-Cre and $Akt1^{f/f};Akt2^{-/-};Akt3^{f/f}$ mice, these two groups served as the control in this study.

The background of the mice used in this study was the C57BL/6 mouse. Both males and females were included. The mice were group-housed in the core animal facility of the Model Animal Research Center at Nanjing University. The temperature in the animal room was kept at $25 \pm 1°C$. The mice had free access to food and water and were kept under a 12 light/dark cycle in the animal room. Mouse breeding was conducted under an Institutional Animal Care and Use Committee-approved animal protocol. All the experiments were performed in accordance with the *Guide for the Care and Use of Laboratory Animals* of Nanjing University.

Nissl staining. Sagittal brain sections at the thickness of 10 µm were used. The method was described previously (Wang et al., 2017). In brief, sections were deparaffinized with xylene and then rehydrated using a series of degraded ethanol. Sections were incubated in 0.5% cresyl violet for 10 min and then washed with PBS. Sections were dehydrated using an ascending series of ethanol. Three sections (spaced at 200 µm) per mouse were chosen for Nissl staining. A microscope (model BX53, Olympus) was used to capture images, and ImageJ was used for quantification. First, to measure the thickness of the cortex, three vertical lines to the pia in the cortex were drawn randomly and then processed by ImageJ. Values were averaged across sections. Second, to measure the area of the fimbria, the latter was outlined according to different cell density between the stratum oriens of the CA3 and the fimbria. Values were averaged across sections for each mouse. Third, in images with high magnifications, the CC could be clearly recognized from the GM of the cortex. Three vertical lines to the boundary of the CC were drawn randomly to measure the thickness of the CC. Values were then averaged for each section. Fourth, since cell density and cell morphology were distinct between WM and GM in the spinal cord (SC), the WM could be readily outlined for area measurement. Values were averaged across sections.

Cortex and spinal cord lysate preparations. Akt cTKO mice were killed at postnatal day 4 (P4) and P14. The cortex and the SC were separately collected and stored at −80°C until use. The CC was included in the cortex when cortical lysates were prepared. Tissues were homogenized in cold radioimmunoprecipitation assay lysis buffer [consisting of the following (in mM): 20 mM Tris-HCl, pH 7.4, 150 mM NaCl, 1 mM EDTA, 1% NP-40, 0.5% sodium deoxycholate, and 0.1% SDS] containing protease inhibitors (5 µg/ml aprotinin, 5 µg/ml leupeptin, 5 µg/ml pepstatin, 1 mM PMSF) and phosphatase inhibitors [10 mM sodium pyrophosphate, 1 mM sodium orthovanadate, 5 µM cantharidin, 5 nM microcystin and 25 µM (–)-p-bromotetramisole oxalate]. Lysates were cleared by centrifugation (14,000 rpm for 20 min). Protein concentration was analyzed using a standard BSA method described previously (Xu et al., 2017).

Table 1. Antibody list

Antibodies	Source	Identifier
Rabbit monoclonal anti-pan-Akt	Cell Signaling Technology	Catalog #4691; RRID:AB_915783
Rabbit monoclonal anti-phospho-Akt (Thr308)	Cell Signaling Technology	Catalog #4056; RRID:AB_331163
Rat monoclonal anti-Ctip2	Abcam	Catalog #ab18465; RRID:AB_2064130
Rabbit monoclonal anti-Tbr1	Abcam	Catalog #ab31940; RRID:AB_2200219
Rabbit monoclonal anti-DYKDDDDK Tag	Cell Signaling Technology	Catalog #14793; RRID:AB_2572291
Rabbit polyclonal anti-HA tag	Abcam	Catalog #ab9110; RRID:AB_307019
Mouse monoclonal anti-GAPDH	CW Biosciences	Catalog #cw0100; RRID: N/A
Rabbit polyclonal anti-β-actin	GenTex	Catalog #CTX124212; RRID: N/A
Mouse monoclonal anti-CC1	Calbiochem	Catalog #op-80; RRID:AB_2057371
Mouse monoclonal anti-GFAP	Santa Cruz Biotechnology	Catalog #sc-65343; RRID:AB_783553
Goat polyclonal anti-Mag	Santa Cruz Biotechnology	Catalog #sc-9543; RRID:AB_670103
Rat monoclonal anti-Mbp	Millipore	Catalog #MAB386; RRID:AB_94975
Rabbit polyclonal anti-Myrf	ABclonal	Catalog #A16355; RRID:AB_2770507
Rabbit polyclonal anti-NeuN	Millipore	Catalog #ABN78; RRID:AB_10807945
Mouse monoclonal anti-Olig2	Millipore	Catalog #MABN50; RRID:AB_10807410
Rabbit monoclonal anti-Pdgfrα	Cell Signaling Technology	Catalog #3174; RRID:AB_2162345
Rabbit monoclonal anti-Sox10	Abcam	Catalog #ab155279; RRID:AB_2650603
Mouse monoclonal anti-Plp1	Millipore	Catalog #MAB388; RRID:AB_177623
Mouse monoclonal anti-synaptophysin (SVP38)	Sigma-Aldrich	Catalog #S5768; RRID:AB_477523
Rabbit monoclonal anti-Fox01	Cell Signaling Technology	Catalog #2880; RRID:AB_2106495
Rabbit anti-phospho-Fox01 (Ser256)	ABclonal	Catalog #AP0172; RRID:AB_2771120
Rabbit anti-phospho-Fox01 (Ser256)	Cell Signaling Technology	Catalog #9461; RRID:AB_329831
Mouse monoclonal anti-PSD95	Millipore	Catalog #MABN68; RRID:AB_10807979

Western blotting. Normalized samples (40 µg total protein) were loaded and transferred to nitrocellulose membrane, which was blocked using 5% (w/v) skim milk for 1 h, incubated with primary antibodies overnight, and reacted with infrared dye-coupled secondary antibodies (various types of IRdye800 and IRdye680). Membranes were scanned using the Odyssey Infrared Imaging System (LI-COR). The antibodies used are listed in Table 1.

Immunohistochemistry. Brain and SC were dissected out and fixed in 4% paraformaldehyde (PFA) overnight. The tissues were then dehydrated in a graded ethanol series and embedded in paraffin. Sections were deparaffinized, rehydrated, blocked in 10% normal goat serum for 30 min, and immunostained with primary antibodies overnight at 4°C. Sections were incubated with secondary antibodies conjugated to Alexa Fluor 488 (1:500; Jackson ImmunoResearch), Cy3 (1:500; Jackson ImmunoResearch), or Cy5 (1:500; Jackson ImmunoResearch). Nuclei were counterstained with DAPI (1 µg/ml; catalog #D9542, Sigma-Aldrich). Images were analyzed with a laser confocal microscope (model TCS SP5, Leica) or a fluorescence microscopy system (model BX53, Olympus). The antibodies used are listed in Table 1.

TUNEL assay. The BrightGreen Apoptosis Detection Kit (Vazyme) was used for TUNEL terminal deoxynucleotidyl transferase-mediated biotinylated UTP nick end labeling) assay. Brain sections were treated with the BrightGreen Apoptosis Detection Kit at 37°C for 1 h, and nuclei were counterstained with DAPI. Fluorescence images were captured using a confocal laser scanning microscope (model SP5, Leica).

BrdU labeling. For BrdU pulse labeling, mice were injected intraperitoneally with BrdU (100 µg/g; catalog #B5002, Sigma-Aldrich) for 3 consecutive days from P7 to P9. Brain and SC samples were collected at P14. Three sections spaced at 200 µm from each brain were stained with antibody against BrdU.

Transmission electron microscopy. P14 mice were perfused with PBS followed by 2% glutaraldehyde and 4% PFA in 0.1 M phosphate buffer. The SC and the optic nerve (ON) were dissected out and postfixed in 2.5% glutaraldehyde in 0.1 M overnight at 4°C. Tissues were rinsed in PBS, postfixed in 1% OsO4 in PBS for 1.5 h, dehydrated in a graded acetone series, and embedded in a Poly/Bed812 resin. Ultrathin sections (60–80 nm) were stained with 1% uranyl acetate and lead citrate and were visualized using an electron microscope (model HT7650, Hitachi). Three transmission electron microscopy (EM) images were used for counting myelinated and nonmyelinated axons per mouse ($n = 3$ mice/ group).

Cell purification by FACS. The *mTmG* reporter was used to generate $Akt1^{f/+};Akt2^{+/-};Akt3^{f/+};Olig1$-$Cre;mTmG$ (control) and $Akt1^{f/f};Akt2^{-/-};Akt3^{f/f};Olig1$-$Cre;mTmG$ (Akt cTKO) mice for cell sorting. Tissues containing the cortex and the CC were dissected out from control and Akt cTKO mice at P4. Meninges were removed in PBS. Tissues were cut into small pieces and incubated in enzyme solution containing 0.1% trypsin and 100 U/ml DNase I for 10 min at 37°C. The tissues were then triturated and filtered with a 70 µm cell strainer and resuspended in PBS at a density of 10^7 cells/ml. Excitation wavelength was set at 488 nm for the argon–ion laser to detect green fluorescent protein (GFP). Debris and small fragments were discarded by the FACS. The sorting speed was 2000–4000 cells/s. GFP$^+$ cells were harvested in ice-cold PBS solution. Fluorescence signals were detected in the FITC (for GFP) and mCherry (for tdTomato) channels by the FACS. Cells positive for tdTomato were collected in the red gate and were non-OPC cells. GFP$^+$ cells collected in the green gate were OPCs.

Primary OPC cultures. A method described previously (Niu et al., 2012a,b) was used. The CC and the cortex in neonatal mice at P2 were dissected and gently triturated. Tissues went through a 40 µm filter to form a single-cell suspension. Cells were plated onto poly-D-lysine-coated dishes (10 cm) in DMEM containing 10% fetal bovine serum and 1% penicillin-streptomycin. When the cultured cells reached 65–75% confluence, the medium was replaced by a serum-free B104 conditional DMEM/F12 (Thermo Fisher Scientific) medium containing 15% B104 CM, 1% N2 (Thermo Fisher Scientific), and 5 µg/ml insulin. For OPC isolation, the medium was replaced by a DMEM/F12 medium containing 0.02% EDTA, 0.5% DNase I, and 5 µg/ml insulin for 15 min at 37°C. The isolated cells then grew in a DMEM/F-12 medium containing 2% B-27 (Thermo Fisher Scientific), 1% N2, PDGF-AA (10 ng/ml; catalog #315–17, PeproTech), and bFGF (10 ng/ml; catalog #100-18B, PeproTech).

Constructs of plasmids. Mouse *Akt3* (gene ID, 23797), *Olig2* (gene ID, 50 913), *Sox10* (gene ID, 20 665), and *Myrf* (gene ID, 225908) were constructed using pLVX vector. Mouse *FoxO1* (gene ID, 56 458) was constructed using pLVX-Flag vector. For the luciferase reporter assay, the promoter region of *Mbp* (gene ID, 17 196), *Sox10*, or *Myrf* was constructed using the pGL3-Luc vector. We designed three luciferase plasmids, which were driven by different fragments of the *Sox10* promoter. These fragments were 212, 557, and 1044 bp, respectively, upstream of the transcriptional start site (TSS).

Mutations in *Olig2* and *FoxO1* were generated using MultiS Fast Mutagenesis Kit (Vazyme), a PCR-based site-directed mutagenesis method. For Olig2-AA, serines at amino acid residues 30 and 115 were

replaced with alanines. Thus, Olig2-AA could not be phosphorylated by Akt. For FoxO1-AAA, it has been shown that the mouse FoxO1 has three Akt-targeted phosphorylation sites, Thr24, Ser253, and Ser316 (Matsuzaki et al., 2005). These three amino acids in FoxO1 were mutated into alanines so that FoxO1 could not be phosphorylated by Akt. Since the Ser253 in the mouse FoxO1 corresponds to the Ser256 in the human FoxO1 (Yamagata et al., 2008), the antibody against human pFoxO1^{Ser256} was used for mouse samples.

Cell culture, transfection, and luciferase reporter assays. N2a (Neuro2a) cells (neuroblastoma cells derived from mouse neural crest) were cultured in DMEM supplemented with 10% FBS and 1% penicillin-streptomycin (Tremblay et al., 2010). N2a cells were seeded and cultured for 1 d at 37°C in the incubator. Transient transfection was performed according to the manufacturer protocol for Lipofectamine 2000 transfection reagent (Thermo Fisher Scientific). N2a cells were transfected with a vector carrying the reporter luciferase together with one expressing Sox10, Myrf, Olig2, Olig2-AA, Akt3, FoxO1, or FoxO1-AAA, respectively. A *CMV* promoter-driven Renilla luciferase was used as the internal control. To inhibit Akt activity, MK2206 was used at a concentration of 5 μM. For Akt activation, insulin was used at a concentration of 1000 ng/ml. The luciferase assay was performed using Dual-Glo (Promega) according to the manufacturer protocol 24 h after transfection. All transfection data are presented from at least three separate experiments (Hou et al., 2021; Wang et al., 2021).

Chromatin immunoprecipitation. For chromatin immunoprecipitation (ChIP) assay, we used the Enzymatic Chromatin IP Kit (Cell Signaling Technology). According to the manufacturer protocol, N2a cells were cross-linked in 1% fresh formaldehyde solution for 10 min at room temperature followed by 125 mM glycine for 5 min. Nuclei were prepared in buffer A on ice for 10 min. The DNAs were then digested by micrococcal nuclease. For immunoprecipitation, one volume of chromatin solution was mixed with four volumes of ChIP buffer. Samples were incubated with 2 μg of antibodies overnight at 4°C. Immunocomplexes were captured by ChIP-Grade Protein G MAGnetic Beads for 2 h at 4°C. The beads were washed three times with low-salt buffer and then once with high-salt buffer. Chromatin was eluted from beads, and the cross-link was reversed by proteinase K at 65°C for 2 h. Finally, the DNAs were purified using spin columns. Quantitative real-time PCRs (qRT-PCRs) were performed using SYBR Green Master Mix with the Applied Biosystems Prism StepOnePlus System (Thermo Fisher Scientific). The enrichment was calculated as $2^{-\Delta Ct}$, where ΔCt (cycle threshold) = Ct (ChIP) – Ct(input). The following Sox10 primers were used for ChIP-qRT-PCR: forward (F), AAGGTTATCCAGCTGCGGTC; and reverse (R), ATCCCACTGAGTCCCA CTGT.

Quantitative real-time PCR. For RNA sample preparations, the CC and the cortex were mixed together. Total RNAs were extracted from CNS subregions or FACS-purified OPCs using TRIzol (Thermo Fisher Scientific). Approximately 1 μg of total RNAs were reverse transcribed with the PrimeScript RT Reagent Kit (Takara Bio) according to manufacturer instructions. qRT-PCR was performed using SYBR Green Supermix Reagent (Genstar) and the Applied Biosystems Prism StepOnePlus System (Thermo Fisher Scientific) with an initial denaturation for 5 min at 95°C, followed by 40 cycles of 10 s of denaturation at 95°C, 30 s of amplification and quantification at 60°C, and a melting curve program. Quantification was performed by the comparative Ct method, using GAPDH as the internal control.

The following was the information for primers used in this study: *Olig2*-F: ACC ACGTGTCGGCTATGG, *Olig2*-R: CCATAATCCCCTA GGCCCAG; *Myrf*-F: TCTAA CCCCAAGCACTCAGG, *Myrf*-R: GT TCTTGGTCTTGCTCTGCC; *Sox10*-F: CAGT ACCCTCACCTCCAC AA, *Sox10*-R: CGCCGAGGTTGGTACTTGTA; *Mag*-F: CAG ATCC TAGCCACGGTCAT, *Mag*-R: CACACATAGACACTGCACGG; *Mbp*-F: TCAC ACACGAGAACTACCCA, *Mbp*-R: TGGTGTTCGAGG TGTCACAA; *Mog*-F: ATGA AGGAGGCTACACCTGC, *Mog*-R: CA AGTGCGATGAGAGTCAGC; *Plp1*-F: TTCC CTAGCAAGACCT CTGC, *Plp1*-R: CCATGAGTTTAAGGACGGCG; *Akt3*-F: AAAC AGAACGACCAAAGCC, *Akt3*-R: CGTCCACTCTTCTCTTTCCT; *Akt1*-F: CAGAC TGTGGCAGATGGACTC, *Akt1*-R: AAACTCGTT CATGGTCACACGG; *Gapdh*-F: G AGTGTTTCCTCGTCCCGT; and *Gapdh*-R: ACAATCTCCACTTTGCCACTG.

Cell counting. Three to six animals per genotype were used for cell-counting experiments. Images for immunohistochemistry (IHC), fluorescence IHC, and TUNEL experiments were captured under the 10× objective of a microscope (model BX53, Olympus). Two to four sections per animal spaced at 200 μm were used for counting purposes. Images normally covered the following CNS subregions: the CC, the striatum, the motor cortex, and the SC. ImageJ was used to count CC1$^+$, Pdgfrα^+, and Sox10$^+$ cells, and to measure the area for various CNS subregions.

Experimental design and statistical analyses. Data were presented as the mean ± SEM. A two-tailed Student's *t* test was performed to examine the difference between control and *Akt* cTKO mice; $p < 0.05$ was considered as significant. Since phenotypes were highly homogeneous in *Akt* cTKO mice, three to five pairs of mice were used for cell counting and statistical analyses. For multiple comparisons, we performed one-way ANOVA followed by Tukey–Kramer *post hoc* test, and $p < 0.05$ was considered as significant. Statistical analyses were performed with Microsoft Excel or GraphPad Prism 5.

Results

WM development is deficient in *Akt* cTKO mice

Since germ-line deletion of Akt three isoforms leads to embryonic lethality in mice (Dummler and Hemmings, 2007; Wang et al., 2015), we sought to generate viable *Akt* cTKO mice. *Akt1$^{f/f}$* and *Akt2$^{-/-}$* mice were reported by us previously (Wang et al., 2015). We generated floxed *Akt3* mice using a gene-targeting strategy similar to that used for *Akt1$^{f/f}$* (Fig. 1A,B). We obtained control and *Akt* cTKO mice through multiple breeding steps. To visualize the expression pattern of the Cre recombinase, the *mTmG* mouse (Muzumdar et al., 2007) was crossed with the *Olig1-Cre* mouse (Lu et al., 2002). GFP-expressing cells were abundantly observed in the CC and the cortex in *Olig1-Cre; mTmG* mice at P0 (Fig. 1C).

To determine inactivation efficiency of Akt, FACS technique was used to collect GFP$^+$ cells from tissues containing the CC and the cortex. Quantification by the FACS system revealed no significant differences on the total number of cells collected and the ratio of GFP$^+$ cells to total cells between control (*Akt1$^{f/+}$*; *Akt2$^{+/-}$;Akt3$^{f/+}$;Olig1-Cre;mTmG*) and *Akt* cTKO (*Akt1$^{f/f}$*; *Akt2$^{-/-}$;Akt3$^{f/f}$;Olig1-Cre;mTmG*) mice at P4 (Fig. 1D). We used GFP$^+$ cells collected by the FACS to prepare RNA samples for qRT-PCR analysis, which showed very low RNA levels for *Akt1* and *Akt3* in the cTKO compared with the control (Fig. 1E). Moreover, we cultured OPCs from cortices of *Akt* cTKO mice at P2. Double staining of Olig2/Akt showed that Olig2$^+$ cells were largely negative for total Akt (Fig. 1F).

Compared with littermate controls, *Akt* cTKO mice started to show tremor, seizure, and ataxia at approximately P12, reminiscent of phenotypes for myelin-deficient mice (Emery et al., 2009; Weng et al., 2012). We found that none of the *Akt* cTKO mice lived >3 weeks (Fig. 2A), indicating a short life span. Although the low survival rate in *Akt* cTKO mice may involve complicated mechanisms, we reasoned that severe seizure may account for the early death of *Akt* cTKOs. We found that the brain size was comparable between control and *Akt* cTKO mice (Fig. 2B). However, the SC and the ON were translucent in mutants (Fig. 2C,D), suggesting a loss of lipid contents. Nissl staining showed that the size of the cortex or the hippocampus was not different between control and *Akt* cTKO mice at P14 (Fig. 2E,F). In contrast, the WM subregions were changed in *Akt* cTKO mice. First, the fimbria was smaller in *Akt* cTKO mice than in controls (Fig. 2G,H). Second, the thickness of the CC was significantly reduced in *Akt* cTKO mice compared with controls (Fig. 2I,J). Third, the area for the WM of the SC was significantly decreased in *Akt* cTKO mice (Fig. 2K,L).
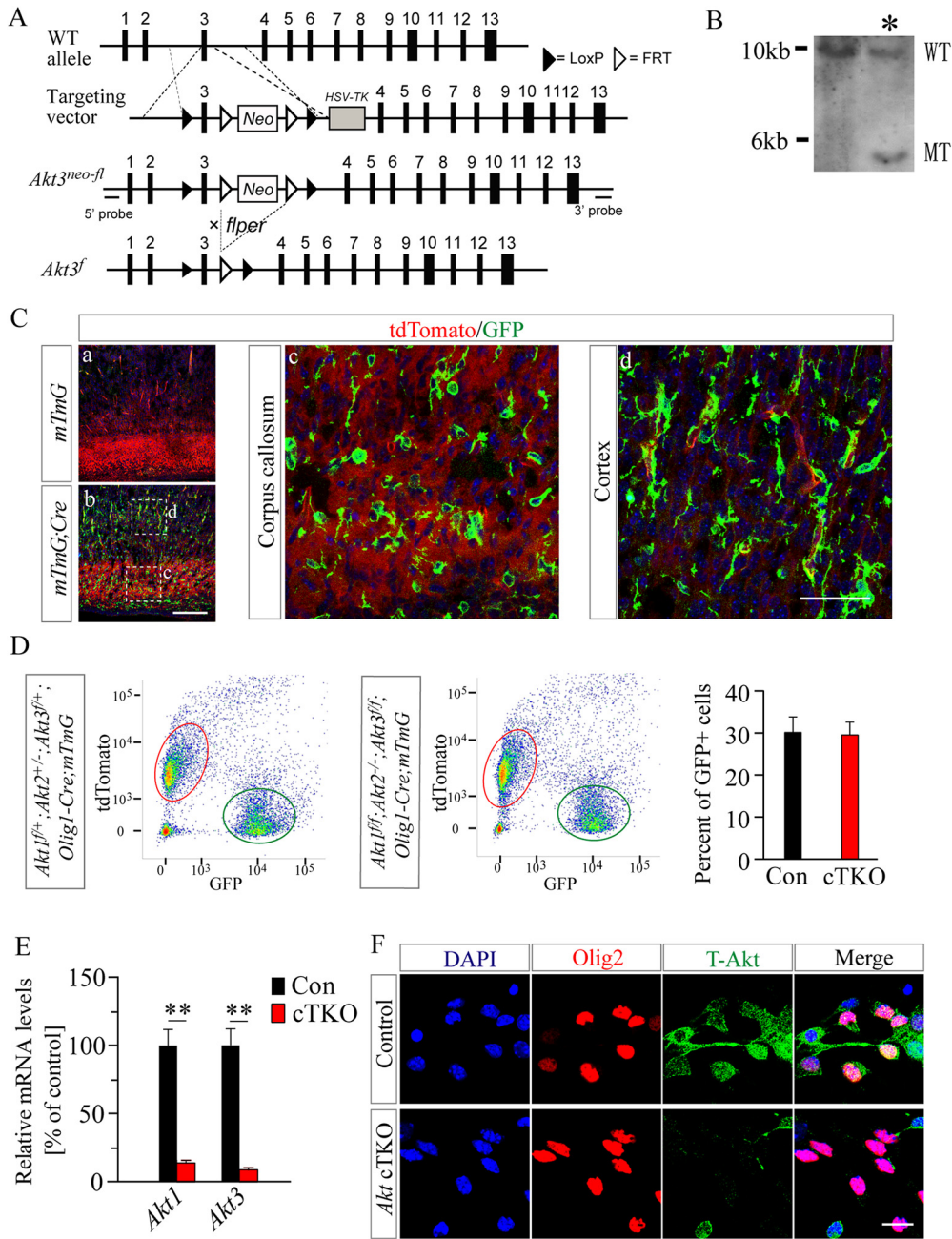
Figure 1. Generation of OL lineage cell-specific *Akt* cTKO mice. ***A***, Gene-targeting strategy for the generation of floxed *Akt3* mice. In the targeting vector, a *Neo* resistance cassette, *FRT* (open triangle), and two *LoxP* (solid triangle) sites were shown. *HSV-TK* was used for negative selection. *Akt3^{fln/+}* mice were bred with a *flper* mouse to remove the *Neo* cassette to generate *Akt3^{f/+}*. ***B***, Southern blotting. The proper homologous recombination in ES cells (∗) was confirmed by the presence of the mutant (MT) allele for *Akt3*. ***C***, Analysis on the expression pattern of Cre. Brain sections were prepared from *mTmG* (***a***) and *mTmG;Olig1-Cre* (***b***) mice at P0. Cre-mediated GFP expression was observed in OPCs in the CC (***c***) and the cortex (***d***) in *mTmG;Olig1-Cre* mice. Scale bars: ***b***, 200 μm; ***d***, 50 μm. ***D***, Purification of OPCs by FACS. Tissues from the cortex and the CC were mixed up for cell sorting. Control (*Akt1^{f/+};Akt2^{+/−};Akt3^{f/+};Olig1-Cre;mTmG*) and *Akt* cTKO (*Akt1^{f/f};Akt2^{−/−};Akt3^{f/f};Olig1-Cre;mTmG*) mice at P4 were used. There was no significant difference on the ratio of GFP$^+$ cells to total cells between these two genotypes (control, n = 7; cTKO, n = 10; $p > 0.9$). ***E***, Q-RT-PCR analysis on *Akt1* and *Akt3*. RNA samples were prepared from GFP$^+$ cells collected for ***D***. There were significant differences on relative levels of *Akt1* and *Akt3* between control (*Akt1^{f/+};Akt2^{+/−};Akt3^{f/+};Olig1-Cre;mTmG*) and *Akt* cTKO (*Akt1^{f/f};Akt2^{−/−};Akt3^{f/f};Olig1-Cre;mTmG*; n = 4 mice/group; ∗∗$p < 0.01$; two-tailed student *t* test). ***F***, Double staining for Olig2 and Akt in OPC cultures. Olig2$^+$ cells were positive for total Akt in control cultures but negative in *Akt* cTKOs. Scale bar, 15 μm.

Loss of total Akt blocks OL differentiation in the CNS

Next, various markers were used to analyze myelin phenotypes. First, fluorescence IHC was conducted. We observed intense immunoreactivity of Mbp in the SC, the cortex, the CC, and the cerebellum in control mice at P14 (Fig. 3A). In contrast, Mbp was hardly detected in these areas in *Akt* cTKO mice (Fig. 3A). Similar results were obtained for Plp1 (Fig. 3B). Interestingly, few Mbp$^+$ and Plp1$^+$ cells were detected in the SC of *Akt* cTKO

mice (Fig. 3A,B). One possibility was that not all OPCs in the SC of *Olig1-Cre* mice expressed Cre. Thus, a very small proportion of Cre$^-$ OPCs may be able to differentiate to mature OLs in the SC of *Akt* cTKO mice. Second, proteins for Mbp, Plp1, and MAG were hardly detected by Western blotting in cortical and SC samples from P14 *Akt* cTKO mice compared with controls (Fig. 3C,D). Third, levels for *Mbp*, *Mag*, *Mog*, and *Plp1* mRNAs were undetectable in the cortex and the SC in *Akt* cTKO mice
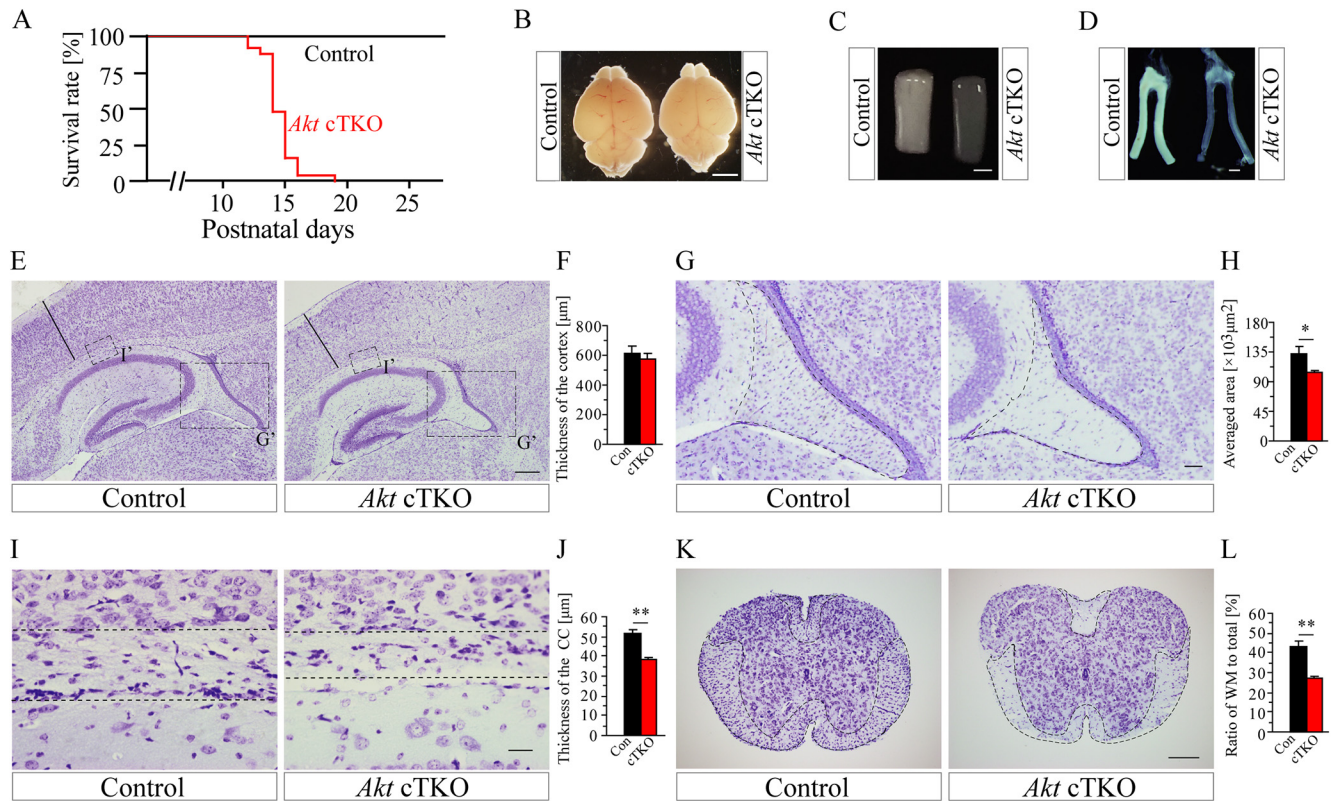
Figure 2. Deficient white matter development in *Akt* cTKO mice. *A*, Survival rate of *Akt* cTKO mice. All *Akt* cTKO mice died before P20. A total of 50 mice ($n = 25$/group) were tested. *B–D*, Photographs for brain, spinal cord, and optic nerve in P14 mice. *B*, The size of the brain was visually not different between control and *Akt* cTKO mice. *C, D*, The spinal cord (*C*) and the optic nerve (*D*) were translucent in *Akt* cTKO mice. Scale bars: *B*, 2 mm; *C*, 1 mm; *D*, 200 μm. *E–L*, Morphologic analyses on different CNS regions by Nissl staining. Boxed areas G' and I' in *E* were enlarged as images in *G* and *I*, respectively. There was no difference on the thickness of the cortex or the size of the hippocampus between control and *Akt* cTKO mice (*E, F*). There was a significant difference in the area of the fimbria (*G, H*), the CC (*I, J*), and the white matter of the SC (*K, L*) between control and *Akt* cTKO mice. Scale bars: *E*, 200 μm; *G*, 50 μm; *I*, 20 μm; *K*, 100 μm. $n = 4$ mice/group. $*p < 0.05$; $**p < 0.01$; two-tailed student *t* test.

(Fig. 3*E*). Finally, we used the EM technique to examine myelin structure. Compared with control mice at P14, *Akt* cTKOs exhibited no myelinated axons in the SC and ON (Fig. 3*F,G*), suggesting that loss of total Akt prevents the formation of myelin sheath.

To study whether OLs and OPCs in *Akt1*$^{f/+}$;*Akt2*$^{+/-}$;*Akt3*$^{f/+}$; *Olig1-Cre* mice were different from those in *Akt1*$^{f/f}$;*Akt2*$^{-/-}$; *Akt3*$^{f/f}$ mice, CC1 (Fig. 4*A*) and Pdgfrα (Fig. 4*B*) were used for IHC experiments using brain sections at P14. Quantification results revealed no significant difference in the number of CC1$^+$ or Pdgfrα^+ cells between these two groups (Fig. 4*C*). These findings suggest that heterozygous knockout of three Akt isoforms in OL lineage cells does not impair the population of OLs and OPCs. Next, we examined OLs in *Akt* cTKO mice by performing IHC on CC1. CC1$^+$ cells were not observed in the CC and the SC in *Akt* cTKO mice at P7 and P14 (Fig. 4*D–G*). Control mice at P7 had few CC1$^+$ cells in the CC and the SC compared with those at P14 (Fig. 4*D–G*). Overall, *Akt* cTKO mice exhibited a complete loss of mature OLs.

To test the possibility that OL differentiation may be affected by the loss of Akt, we performed BrdU birth-dating experiments. BrdU was injected into mice aged at P7 for 3 consecutive days. BrdU$^+$/CC1$^+$ cells were readily seen in control mice at P14 (Fig. 4*H*). We found that BrdU$^+$/CC1$^+$ cells were not detected and that the ratio of BrdU$^+$/CC1$^+$ cells to BrdU$^+$ cells was almost none in *Akt* cTKO mice (Fig. 4*I*). Statistical analysis confirmed a significant difference in the ratio of BrdU$^+$/CC1$^+$ cells to BrdU$^+$ cells between two genotypes (Fig. 4*I*). Thus, Akt was critical for OL differentiation.

Loss of total Akt causes reduced number of OPCs
To investigate whether deletion of Akt affected OPC development, we conducted histochemical analyses on Pdgfrα and Olig2 using brain and SC sections at P0, P7, and P14 (Fig. 5*A–D*). First, the number of Pdgfrα^+ cells in the CC was not changed in *Akt* cTKO mice at P0 and P7 compared with controls, but it was significantly decreased at P14 (Fig. 5*E*). Second, the number of Pdgfrα^+ cells in the SC was significantly reduced at P7 and P14 but not at P0 (Fig. 5*E*). Third, the number of Olig2$^+$ cells in the CC or the SC was significantly less in *Akt* cTKO mice than in controls at P7 and P14 but not at P0 (Fig. 5*F*).

To find out why the population of OPCs was reduced in *Akt* cTKOs, we performed BrdU pulse-labeling experiments, in which BrdU was injected into pups at P7 and brain sections were prepared 2 h after. We performed double staining of Pdgfrα/ BrdU and then counted Pdgfrα^+/BrdU$^+$ cells in the CC (Fig. 5*G*). We found that the ratio of Pdgfrα^+/BrdU$^+$ cells to Pdgfrα^+ cells was significantly decreased in *Akt* cTKO mice compared with controls (Fig. 5*H*). Moreover, the number of Pdgfrα^+/BrdU$^+$ cells was less in *Akt* cTKO mice than in controls (Fig. 5*I*). Together, these results suggest that loss of total Akt impairs the OPC population by affecting the proliferation of OPCs.

Normal neuronal development and unchanged apoptosis in *Akt* cTKO mice
Since a wealth of evidence has shown that OPCs may be able to differentiate into OLs, astrocytes, and motor neurons (Lu et al.,
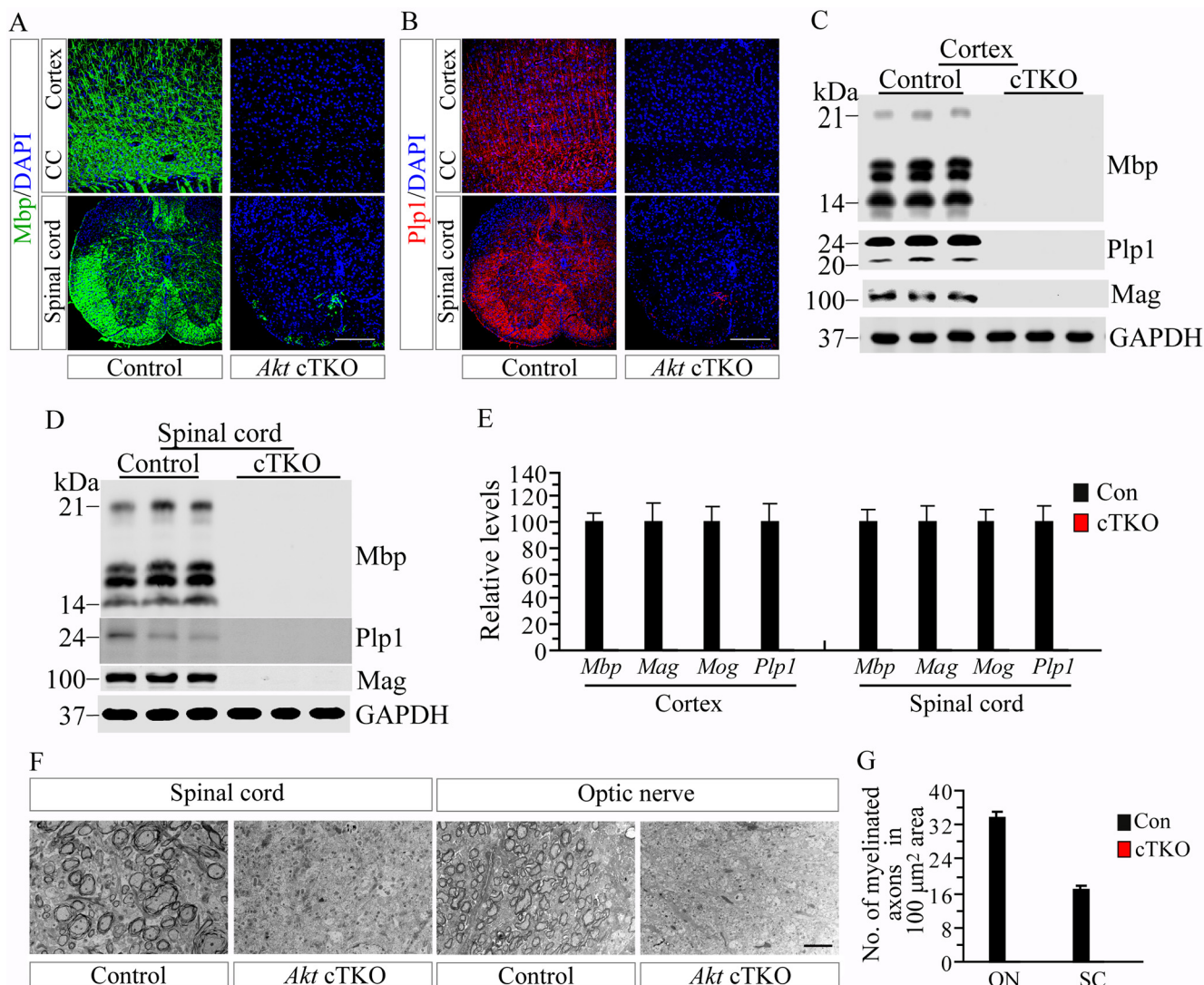
Figure 3. Myelin loss in *Akt* cTKO mice. **A, B,** Representative fluorescence IHC images for Mbp (**A**) and Plp1 (**B**) in the SC, the CC, and the cortex in mice at P14. The immunoreactivity for Mbp (**A**) or Plp1 (**B**) was hardly detected in P14 *Akt* cTKO mice compared with littermate controls. Scale bar, 200 μm. **C, D,** Western blotting on Mbp, Plp1, and Mag. These proteins were not detected in the cortex (**C**) and the SC (**D**) in *Akt* cTKO mice at P14. **E,** qRT-PCR analysis. Levels for *Mbp*, *Mag*, *Mog*, and *Plp1* mRNAs were undetectable in the cortex and the SC in *Akt* cTKO mice at P14. **F,** Electron microscopy analysis. There were no myelinated axons in the SC and the ON in *Akt* cTKO mice at P14. Scale bar, 2 μm. **G,** Averaged number of myelinated axons. There was significant difference on the total number of myelinated axons in the SC and the ON between control and *Akt* cTKO mice at P14. $n = 3$ mice/group. ****$p < 0.001$; two-tailed student t test.

2002; Cai et al., 2007; Zhu et al., 2008; Silbereis et al., 2014; Zhang et al., 2016; Sun et al., 2019), we examined whether other types of cells were also significantly affected in *Akt* cTKO mice. First, IHC on Ctip2/Tbr1 revealed that cortical layers II–IV, V, and VI were comparable between control and *Akt* cTKO mice at P14 (Fig. 6A), suggesting unimpaired cortical lamination. Second, the immunoreactivity of NeuN in the cortex and the SC was not changed in *Akt* cTKO mice at P14 (Fig. 6B,C). Third, the immunoreactivity of GFAP was not different in the cortex (Fig. 6D) and the SC (Fig. 6E) between control and *Akt* cTKO mice at P14. However, it was increased in the hippocampus in *Akt* cTKO mice (Fig. 6D), indicating the activation of astrocytes. Previous evidence has shown that seizures may induce rapid astroglial activation in the hippocampus (Shapiro et al., 2008; Yang et al., 2008). Since *Akt* cTKO mice started to display seizures at approximately P12, we reasoned that the activation of astrocytes in the hippocampus was likely because of severe seizures.

Fourth, protein levels for NeuN, synaptophysin (SVP38), postsynaptic density-95 (PSD-95), and GFAP were not significantly changed in the cortex (Fig. 6F) and the SC (data not shown) in *Akt* cTKO mice compared with controls. Overall, conditional deletion of Akt three isoforms in OL lineage cells did not compensate or enhance neuronal differentiation in the cortex, the CC, and the fimbria.

To test whether there was abnormal cell death in *Akt* cTKO mice, we conducted costaining for TUNEL and Olig2 using brain sections at P7 and P14 (Fig. 6G). The *Ppp2ca* cKO mouse at P0 was used as a positive control (Fig. 6H), since it exhibits abundant apoptotic cell death (Huang et al., 2020). First of all, TUNEL^{+} cells were not observed in the CC or the SC in control and *Akt* cTKO mice at P7 and P14 compared with the positive control (Fig. 6G,H). Second, TUNEL[+]/Olig2^{+} cells were also not seen in the CC or the SC in *Akt* cTKO mice at P7 and P14 (Fig. 6G). Thus, the absence of OLs and the reduction in OPCs in *Akt* cTKO mice were not because of apoptosis.
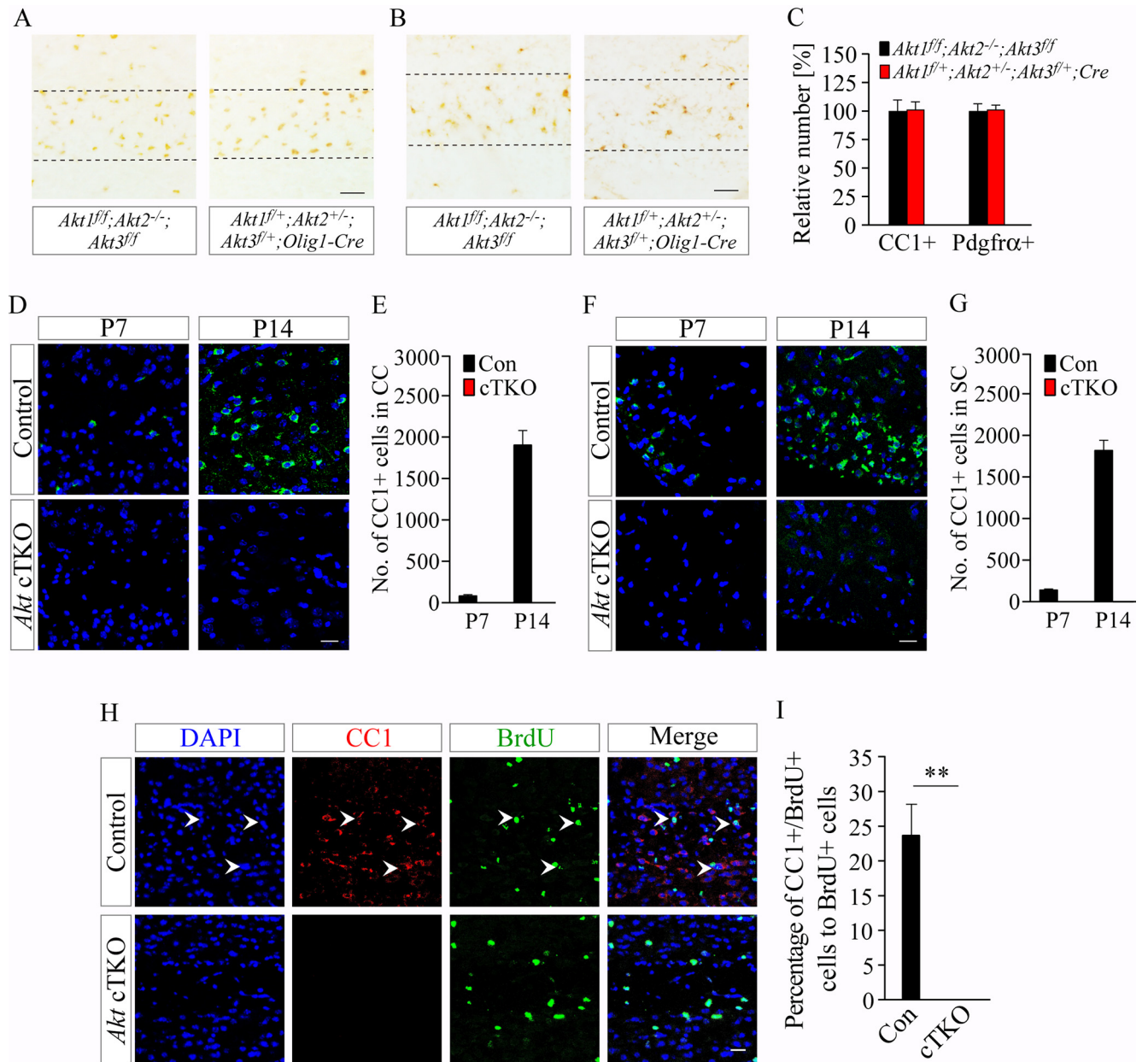
Figure 4. Complete loss of OL differentiation in *Akt* cTKO mice. *A*, *B*, Representative fluorescence IHC images for CC1 (*A*) and Pdgfrα (*B*) in the CC in *Akt1*$^{f/f}$*;Akt2*$^{−/−}$*;Akt3*$^{f/f}$ and *Akt1*$^{f/+}$*; Akt2*$^{+/−}$*;Akt3*$^{f/+}$*;Olig1-Cre* mice at P14. Scale bar, 20 μm. *C*, Relative number of CC1$^+$ and Pdgfrα$^+$ cells. There was no significant difference in relative number of CC1$^+$ or Pdgfrα$^+$ cells between *Akt1*$^{f/f}$*;Akt2*$^{−/−}$*;Akt3*$^{f/f}$ and *Akt1*$^{f/+}$*;Akt2*$^{+/−}$*;Akt3*$^{f/+}$*;Olig1-Cre* mice ($p > 0.6$; $n = 3$–4 mice/group). *D*, *F*, Representative fluorescence IHC images of CC1 in the CC (*D*) and the SC (*F*) in mice at P7 and P14. CC1$^+$ cells were not observed in *Akt* cTKO mice. Scale bar, 20 μm. *E*, *G*, Number of CC1$^+$ cells (per square millimeter area) in the CC (*E*) and the SC (*G*). There was highly significant difference between control and *Akt* cTKO mice ($p < 0.01$; $n = 3$–4 mice/group). *H*, Representative images for double staining of CC1/BrdU in the CC in mice at P14. BrdU was intraperitoneally injected into mice at P7, P8, and P9. Brain sections were collected at P14. White arrowheads indicate CC1$^+$/BrdU$^+$ cells in the CC of control mice but not *Akt* cTKOs. Scale bar, 20 μm. *I*, Percentage of CC1$^+$/BrdU$^+$ cells to BrdU$^+$ cells in the CC. There were no CC1$^+$/BrdU$^+$ cells in *Akt* cTKO mice. $p < 0.01$; $n = 3$–4 mice/group.

Loss of total *Akt* causes downregulation of Sox10 and Myrf in the CNS

It is well known that Sox10 and Olig2 are key TFs to control OL development (Britsch et al., 2001; Lu et al., 2002; Stolt et al., 2002), and that Olig2 may regulate *Sox10* expression via a distant enhancer of *Sox10* (Werner et al., 2007; Küspert et al., 2011). To study whether these two TFs were affected, we conducted Western blot analyses using protein samples prepared from the cortex and the CC. Whereas levels for Sox10 and Olig2 were decreased in *Akt* cTKO mice at P14 compared with littermate controls, those of Sox10, but not Olig2, were decreased in *Akt* cTKOs at P4, an age when mature OLs have not been detected in

the above brain subregions (Fig. 7A–C). Moreover, qRT-PCR data confirmed significant reduction on *Sox10* mRNA levels in RNA samples prepared from mixed tissues of the cortex and the CC in *Akt* cTKO mice at P4 as well as P14 (Fig. 7D), suggesting that Akt may be important for the expression of Sox10, but not Olig2, in OPCs. Next, double staining for Olig2/Sox10 showed robust changes on the immunoreactivity of Sox10 in Olig2$^+$ cells in *Akt* cTKO mice at P14 compared with age-matched controls (Fig. 7E,F). Cell counting results revealed that the total number of Sox10$^+$/Olig2$^+$ was remarkably reduced in the CC and the SC in P14 *Akt* cTKO mice (Fig. 7E,F, $p < 0.005$).
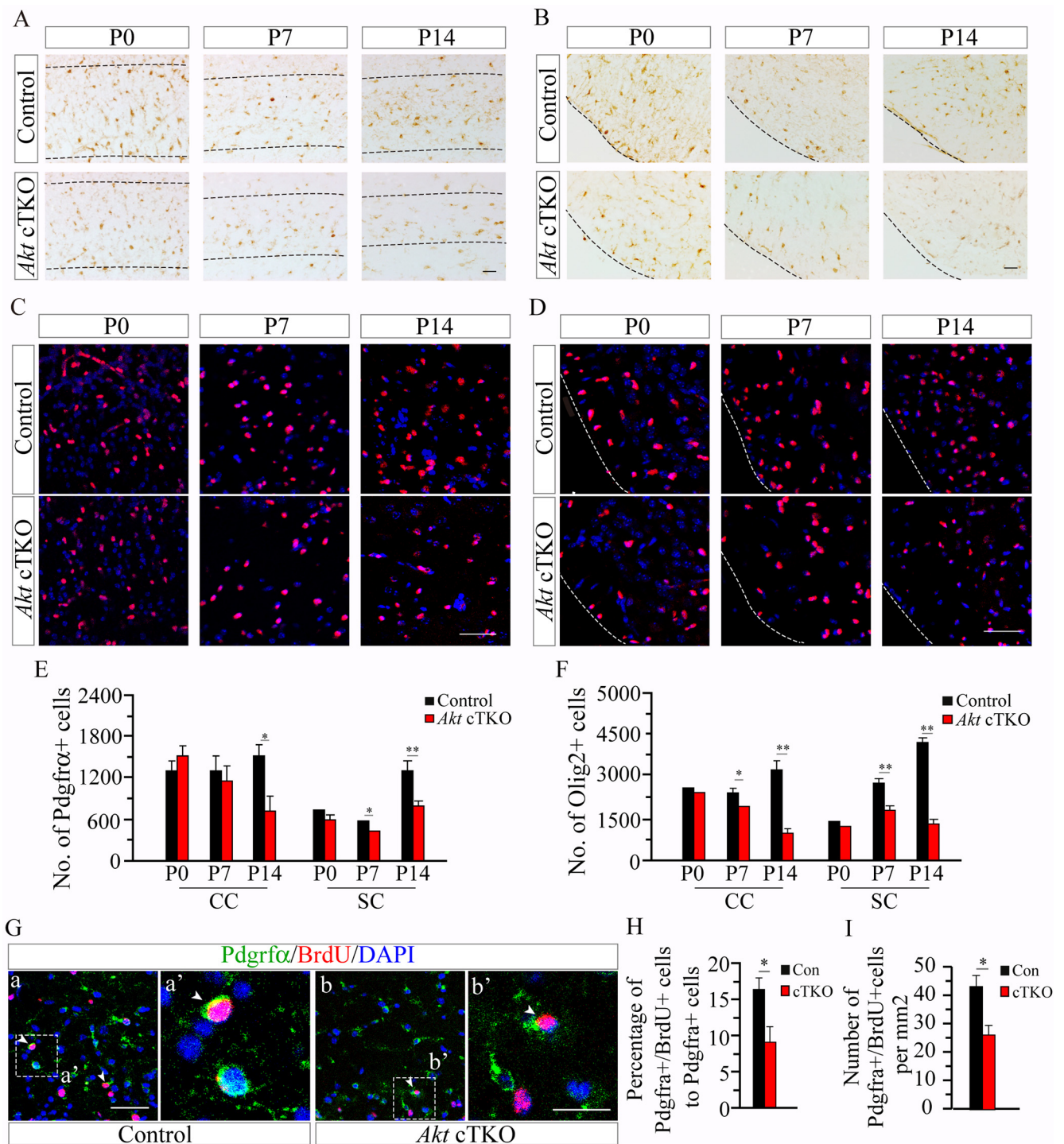
Figure 5. Reduced number of OPCs in *Akt* cTKO mice. *A*, *B*, Representative IHC images of Pdgfrα in the CC (*A*) and the SC (*B*). Brain sections at P0, P7, and P14 were used. Scale bar, 20 μm. *C*, *D*, Representative fluorescence IHC images of Olig2 in the CC (*C*) and the SC (*D*). Brain sections at P0, P7, and P14 were used. Scale bar, 20 μm. *E*, The total number of Pdgfrα^{+} cells in the CC and the SC. There were significant differences between control and *Akt* cTKO mice. $n = 3$–4 mice/group/age. ∗$p < 0.05$; ∗∗$p < 0.01$. *F*, The total number of Olig2^{+} cells in the CC and the SC. There were significant differences between control and *Akt* cTKO mice. $n = 3$–4 mice/group/age. ∗$p < 0.05$; ∗∗$p < 0.01$. *G*, Representative images for double staining of Pdgfrα/BrdU in the CC. Brain sections at P7 were used. Scale bar, 50 μm. *H*, Percentage of Pdgfrα[+]/BrdU^{+} cells to Pdgfrα^{+} cells in the CC. There was significant difference between control and *Akt* cTKO mice. $n = 3$–4 mice/group. ∗$p < 0.05$. *I*, Averaged number of Pdgfrα[+]/BrdU^{+} cells per 1 mm[2] area in the CC. There was a significant difference between control and *Akt* cTKO mice. $n = 3$–4 mice/group. ∗$p < 0.05$.

As a target of Sox10, Myrf is important for OL differentiation (Emery et al., 2009; Elbaz and Popko, 2019). To study whether Myrf was involved in Akt-dependent OL differentiation, we first performed Myrf IHC using *Akt* cTKO brains at P14. There was little immunoreactivity of Myrf in the CC and the SC in *Akt*

cTKO mice compared with controls (Fig. 7G). We then conducted double staining for Olig2 and Myrf. Although the vast majority of Olig2-expressing cells were positive for Myrf in control brain at P14, Olig2^{+}/Myrf^{+} cells were not observed in the CC in *Akt* cTKO mice (Fig. 7H). Moreover, qRT-PCR results
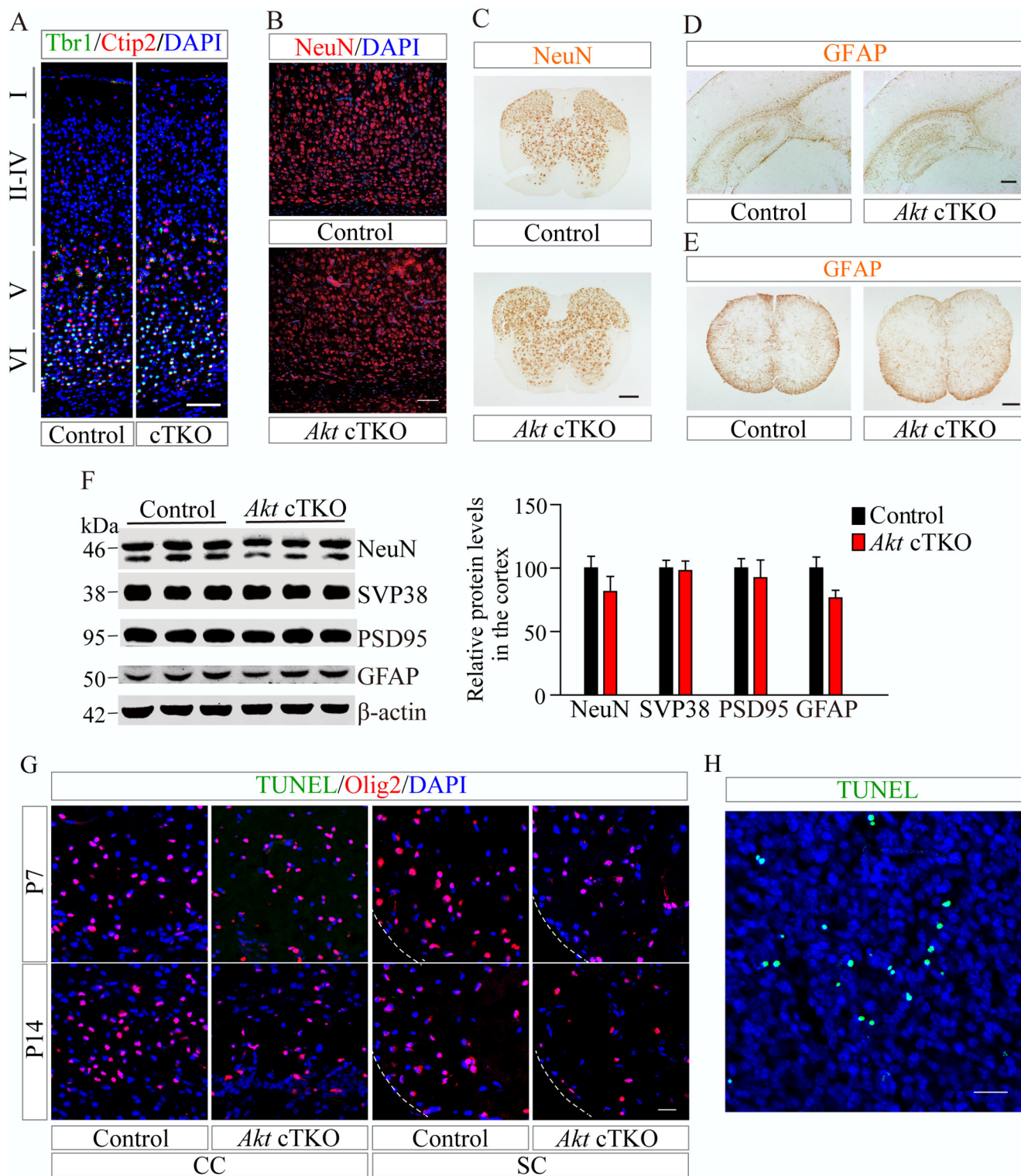
Figure 6. Normal neuronal development in *Akt* cTKO mice. ***A***, Representative images for double staining of Ctip2/Tbr1. There were no abnormalities in Ctip2^{+} and Tbr1^{+} layers in the cortex of *Akt* cTKO mice at P14. Scale bar, 100 μm. ***B***, ***C***, IHC on NeuN. There was no qualitative change on the immunoreactivity of NeuN in the cortex (***B***) and the SC (***C***) in P14 *Akt* cTKO mice compared with controls. Scale bars, 100 μm. ***D***, ***E***, Representative IHC images of GFAP. There was no detectable change on the immunoreactivity of GFAP in the cortex, the CC (***D***) or the SC (***E***) in *Akt* cTKO mice at P14 compared with controls. Scale bars: ***D***, 200 μm; ***E***, 100 μm. ***F***, Western analyses for NeuN, SVP38, PSD-95, and GFAP. There were no significant differences on their levels in the cortex between control and *Akt* cTKO mice at P14. β-Actin served as the loading control. ***G***, Representative images for double staining of TUNEL/Olig2 in the CC and the SC. There were no TUNEL[+] or TUNEL[+]/Olig2^{+} cells in control and *Akt* cTKO mice at P7 and P14. Scale bar, 20 μm. ***H***, Representative image for positive TUNEL staining. A brain section from a *Ppp2cα* cKO mouse at P0 was used as the positive control for the TUNEL assay. Green signals indicate TUNEL^{+} cells. Scale bar, 20 μm.
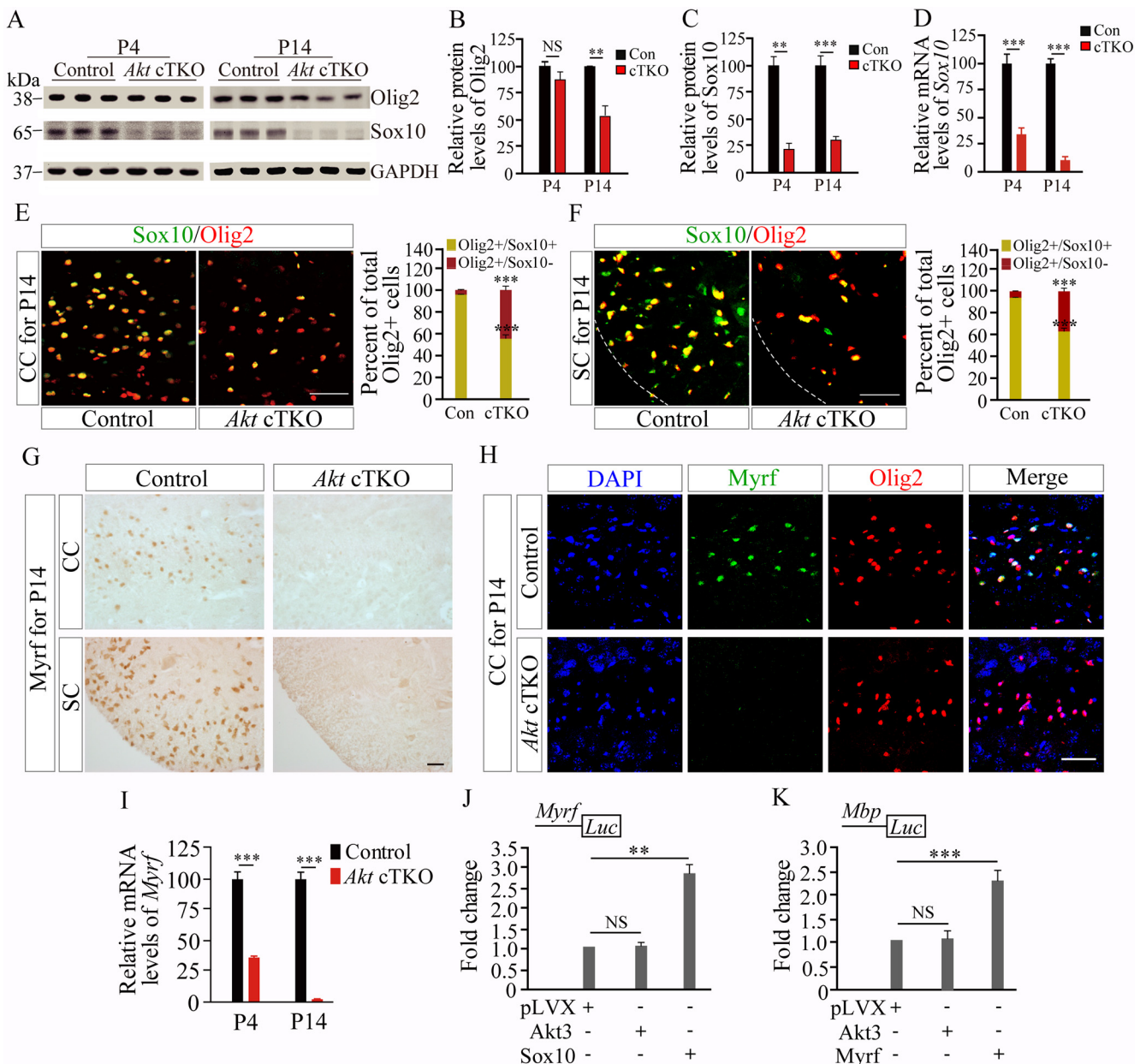
Figure 7. Downregulation of Sox10 and Myrf in *Akt* cTKO mice. *A*, Western blotting for Olig2 and Sox10. Protein samples were prepared from tissues, in which the CC and the cortex were mixed. Control and *Akt* cTKO mice at P4 and P14 were used. GAPDH served as the loading control. *B*, Relative protein levels of Olig2 in the CC and the cortex. There was a significant difference between control and *Akt* cTKO mice at P14 but not at P4 (NS, not significant; ∗∗$p < 0.01$; $n = 3$–4 mice/group; two-tailed student t test). *C*, Relative protein levels of Sox10 in the CC and the cortex. There were significant differences between control and *Akt* cTKO mice at P4 and P14. ∗∗$p < 0.01$; ∗∗∗$p < 0.005$. $n = 3$–4 mice/group; two-tailed student t test. *D*, Relative mRNA levels of *Sox10* in the CC and the cortex. There were significant differences between control and *Akt* cTKO mice at P4 and P14. ∗∗∗$p < 0.005$. $n = 3$–4 mice/group; two-tailed Student's t test. *E*, *F*, Representative images for double staining of Olig2/Sox10 in the CC (*E*) and the SC (*F*). Scale bars, 50 μm. There was significant difference on the ratio of Olig2$^+$/Sox10$^+$ cells to total Olig2$^+$ cells between control and *Akt* cTKO mice in the CC (*E*) and the SC (*F*). ∗∗∗$p < 0.005$. $n = 3$–4 mice/group. *G*, Representative IHC images of Myrf. Myrf was detected in the CC and the SC in control but not *Akt* cTKO mice at P14. Scale bar, 20 μm. *H*, Double staining of Olig2/Myrf. There were abundant Olig2$^+$/Myrf$^+$ cells in the CC and the cortex in control but not *Akt* cTKO mice at P14. Scale bar, 50 μm. *I*, *Myrf* mRNA levels in samples prepared from the CC and the cortex. There was remarkable reduction in *Akt* cTKO mice at P4 or P14. $n = 3$–5/group. ∗∗∗$p < 0.005$; two-tailed student t test. *J*, *K*, Luciferase experiments on Akt3. N2a cells were transfected with a vector carrying *Myrf* (*J*) or *Mbp* (*K*) promoter-driven luciferase reporter together with one expressing Akt3 or Sox10 (*J*) or one expressing Akt3 or Myrf (*K*). *J*, The activity of the *Myrf* promoter was enhanced by Sox10 but not Akt3. *K*, The activity of the *Mbp* promoter was enhanced by Myrf but not Akt3. Values were averaged from three independent experiments. Data represent the mean ± SEM. ∗∗$p < 0.01$; ∗∗∗$p < 0.005$. NS, Not significant. $n = 3$ independent experiments; one-way ANOVA.

revealed dramatically decreased *Myrf* RNA levels in *Akt* cTKO mice at P4 and P14 compared with controls (Fig. 7*I*). Thus, the loss of total Akt caused significant reduction of *Myrf* expression. To test whether Akt could directly regulate *Myrf* or *Mbp* expression, N2a cells were transfected with a vector carrying *Akt3* together with one expressing the *Myrf* promoter-driven luciferase reporter. Unlike Sox10, recombinant Akt3 did not change the promoter activity of *Myrf* (Fig. 7*J*). N2a cells were also transfected with vectors carrying *Akt3* and the *Mbp* promoter-driven luciferase reporter. We found that Myrf, but not Akt3, significantly increased the promoter activity of *Mbp* (Fig. 7*K*). Overall, the loss of total Akt may downregulate Sox10 and Myrf.
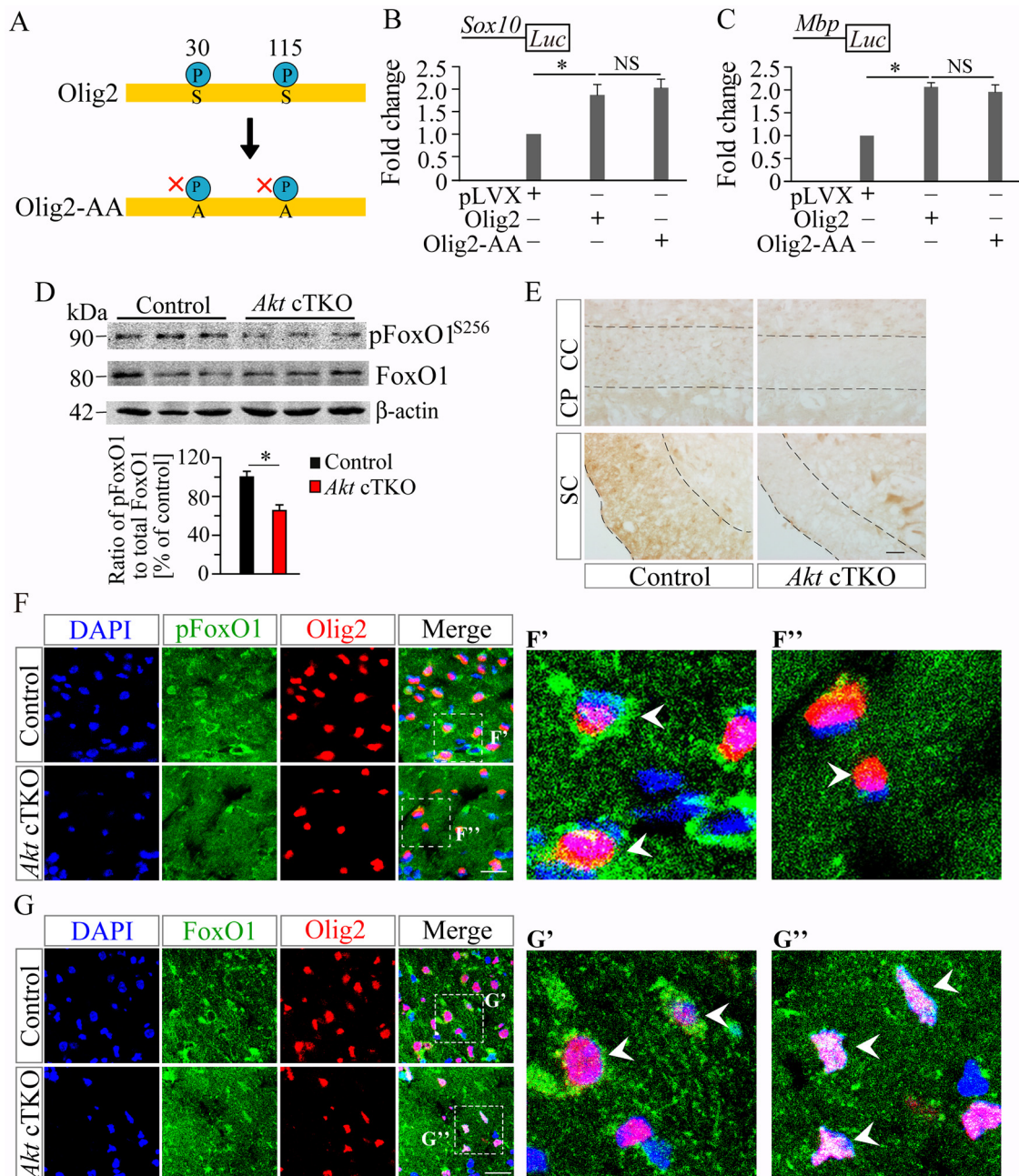
Figure 8. Decreased levels of phosphorylated FoxO1 in *Akt* cTKO mice. *A*, Two serines in WT Olig2 were mutated to alanines (Olig2-AA) to prevent phosphorylation by Akt. *B*, *C*, N2a cells were transfected with a vector carrying *Sox10* (*B*) or *Mbp* (*C*) promoter-driven luciferase reporter together with one expressing Olig2 or Olig2-AA. The luciferase activity was measured 24 h after the transfection. Data represent the mean ± SEM. ∗$p < 0.05$. NS, Not significant. $n = 3$ independent experiments; one-way ANOVA. *D*, Western analyses on total and phosphorylated FoxO1. There was no difference in protein levels of total FoxO1 in the cortex between control and *Akt* cTKO mice at P4. &There was significant difference on the ratio of pFoxO1^{Ser256} to total FoxO1 between two genotypes (∗$p < 0.05$; $n = 4$ mice/group; two-tailed student t test). *E*, Representative images for IHC on pFoxO1^{Ser256}. Abundant pFoxO1$^{Ser256+}$ cells were observed in the CC and the white matter of the SC in control but not *Akt* cTKO mice at P14. In contrast, there were pFoxO1$^{Ser256+}$ cells in the cortex (Ctx) and the caudate putamen (CP) in *Akt* cTKO mice. Scale bar, 40 μm. *F*, *G*, Representative images for costaining of pFoxO1/Olig2 (*F*) and FoxO1/Olig2 (*G*). Brain sections from mice at P14 were used for IHC, and images were captured from the CC area. *F*, The immunoreactivity of pFoxO1^{S256} was absent in *Akt* cTKO Olig2$^+$ cells, and it was present mainly in the cytosol of controls. *G*, FoxO1$^+$ signal was abundantly seen in the nucleus but not the cytosol of *Akt* cTKO Olig2$^+$ cells, and it was detected in the cytosol but not the nucleus of control Olig2$^+$ cells. Boxed areas in *F* and *G* were enlarged as *F′* and *F′′*, and *G′* and *G′′*, respectively. Scale bar, 20 μm.

Phosphorylation of FoxO1 by Akt is critical for Sox10 expression

To understand the molecular mechanisms underlying Akt-dependent Sox10 expression, we conducted *in vitro* experiments. Since previous evidence has shown that the Ser30 in Olig2 is a phosphorylation site for Akt in neural stem cells (Setoguchi and Kondo, 2004), we tested whether phosphorylation of Olig2 by

Akt was important for Sox10 expression. To this end, a mutant Olig2 (referred to as Olig2-AA), in which Ser30 and Ser115 were replaced by alanines, was expressed in N2a cells (Fig. 8A). Luciferase experiments showed that the expression of Olig2-AA did not change the promoter activity of *Sox10* (Fig. 8B) or *Mbp* (Fig. 8C) compared with Olig2 without any mutations. These results suggest that Olig2 may regulate *Sox10* expression via

enhancing the promoter activity, and that phosphorylation of Olig2 by Akt may not be critical.

The FoxO family of TFs plays important roles in multiple cellular processes, including neurogenesis and autophagy (van der Voss and Coffer, 2008; Zhao et al., 2010; Schäffner et al., 2018). Like Olig2, FoxO1 is also a main target of Akt (Brunet et al., 1999). To examine changes on FoxO1 and phosphorylated FoxO1 (pFoxO1) in *Akt* cTKO mice, protein samples were prepared from tissues mixed from the cortex and the CC at P4. Since antibody against mouse pFoxO1^{Ser253} is not commercially available to us, we used an antibody against human pFoxO1^{Ser256} for biochemical and histologic experiments. Western blot analysis revealed a significant reduction in levels of pFoxO1^{Ser256} but not of total FoxO1 in *Akt* cTKO mice compared with controls (Fig. 8D). IHC results showed that cells in the CC and the WM of the SC were negative for pFoxO1^{Ser256} in *Akt* cTKO mice (Fig. 8E).

In addition, we completed two types of double staining using brain sections from control and *Akt* cTKO mice at P14. First, costaining for pFoxO1^{S256} and Olig2 was performed to examine the expression pattern of pFoxO1^{S256}. Whereas the pFoxO1^{S256} immunoreactivity was undetectable in Olig2$^+$ cells in the CC in *Akt* cTKO mice compared with controls (Fig. 8F), it was abundantly present in the cytoplasm of control Olig2$^+$ cells (Fig. 8F). Second, costaining of FoxO1/Olig2 revealed that the FoxO1 immunoreactivity was largely detected in the nucleus of *Akt* cTKO Olig2$^+$ cells (Fig. 8G). Moreover, the immunoreactivity of FoxO1 was undetectable in the nucleus of Olig2$^+$ cells in control mice compared with *Akt* cTKOs (Fig. 8F,G). Thus, the loss of total Akt significantly inhibited phosphorylation of FoxO1.

To determine whether phosphorylation of FoxO1 by Akt could be important for Sox10 expression, three Akt-targeted amino acids were mutated to alanines in FoxO1 (referred to as FoxO1-AAA; Fig. 9A). N2a cells were transfected with plasmids expressing pLVX, FoxO1-AAA, FoxO1, Olig2, Olig2/FoxO1, or Olig2/FoxO1-AAA. First, the expression of FoxO1 did not change the *Sox10* promoter activity, which was 1496 bp upstream of the TSS (Fig. 9B). In contrast, the expression of FoxO1-AAA significantly repressed the *Sox10* promoter activity compared with FoxO1 (Fig. 9B). Second, the expression of Olig2 or Olig2/FoxO1 produced comparable enhancement on the *Sox10* promoter activity (Fig. 9B). However, expression of Olig2/FoxO1-AAA significantly inhibited the *Sox10* promoter activity compared with Olig2/FoxO1 (Fig. 9B). Thus, mutant FoxO1 significantly repressed the *Sox10* promoter activity. These results suggest that phosphorylation of FoxO1 by Akt may be critical for *Sox10* expression.

The following observations were also obtained from the above experiments. First, for plasmids expressing Olig2/FoxO1-AAA and Olig2/FoxO1, FoxO1 was mainly detected in the cytoplasm, but FoxO1-AAA was detected in the nucleus (Fig. 9C). Second, MK2206 (an Akt inhibitor; Hirai et al., 2010) and insulin (for Akt activation; Nakae et al., 1999) were used to treat N2a cells. The latter were transfected with a plasmid expressing Flag-FoxO1. We observed that levels of pAkt^{Thr308} and pGSK3β^{Ser9} were decreased by MK2206 but were increased by insulin (Fig. 9D). Third, IHC results revealed nuclear localization of Flag-FoxO1 after the MK2206 treatment and cytoplasmic localization by insulin (Fig. 9E). Thus, Akt-dependent phosphorylation of FoxO1 triggered its cytoplasmic translocation.

Nonphosphorylated FoxO1 is enriched in the promoter of *Sox10*

To identify which region in the *Sox10* promoter was important for mutant FoxO1 to bind, we constructed three luciferase reporters expressing different fragments of the *Sox10* promoter. The first fragment (Fragment1) was 212 bp upstream of the TSS (Fig. 10A). We found that the expression of FoxO1-AAA did not change the luciferase activity for Fragment1 induced by Olig2 compared with FoxO1 (Fig. 10A). The second fragment (Fragment2) was 557 bp upstream of the TSS (Fig. 10B). We found that the expression of FoxO1-AAA significantly repressed the luciferase activity for Fragment2 induced by Olig2 compared with FoxO1 (Fig. 10B). Similar results were obtained for the third fragment (Fragment3), which covered 1044 bps upstream of the TSS (Fig. 10C).

We then preformed a ChIP–qRT-PCR assay using an antibody against Flag in N2a cells, which were transfected with a vector expressing Flag, Flag-FoxO1, or Flag-FoxO1-AAA. We found that FoxO1-AAA was significantly enriched in the *Sox10* promoter compared with FoxO1 (Fig. 10D). To test whether this *in vitro* finding could be verified at the *in vivo* level, we used FoxO1 antibody to perform ChIP–qRT-PCR experiments on samples that contained the cortex and the CC from control and *Akt* cTKO mice at P7. We observed significantly increased relative enrichment of FoxO1 in the *Sox10* promoter in *Akt* cTKO mice compared with controls (Fig. 10E). Overall, these results suggest that a nonphosphorylated form of FoxO1 may inhibit the promoter activity of *Sox10* via binding to a specific region of the promoter.

To examine the effects of Akt inhibition on Sox10 expression, we used two Akt inhibitors, MK2206 and capivasertib (Cap), to treat primary OPCs cultured from control cortices at P2, respectively. Costaining for Olig2, FoxO1, and Sox10 was then conducted (Fig. 10F). First of all, we found that the FoxO1$^+$ signal was predominantly present in the nucleus of Olig2$^+$/Sox10$^-$ cells in MK2206- or Cap-treated cultures (Fig. 10F). Second, the FoxO1$^+$ signal was hardly seen in the cytoplasm of Olig2$^+$ cells in MK2206- or Cap-treated cultures (Fig. 10F). Third, there was a decreased number of Sox10$^+$ cells in OPC cultures treated with MK2206 or Cap compared those treated with Mock (Fig. 10F). Moreover, we performed costaining of TUNEL/Olig2 in OPC cultures treated with MK2206. However, no significant difference in the ratio of TUNEL$^+$/Olig2$^+$ cells to Olig2$^+$ cells was detected between cultures treated with Mock and MK2206 (Fig. 10G). Moreover, cell-counting data confirmed a significant increase in the number of Olig2$^+$/FoxO1$^+$/Sox10$^-$ cells in OPC cultures treated with MK2206 or Cap (Fig. 10H). These results suggest that pharmacological inhibition of Akt activity may repress Sox10 expression in cultured OPCs.

FoxO1 phosphorylation and OL differentiation are unimpaired in Akt single-isoform knock-out mice

Previous evidence has shown that Akt1, Akt2, and Akt3 contribute to certain amounts of total Akt in the mouse brain, respectively (Easton et al., 2005). Thus, in contrast to OPCs in *Akt* cTKO mice, OPCs in any Akt single-isoform KO line exhibit partial preservation of Akt function. We wondered whether pFoxO1 levels may be restored in *Akt1*$^{-/-}$, *Akt2*$^{-/-}$, and *Akt3*$^{-/-}$ mice. We further tested the hypothesis that the restoration of FoxO1 phosphorylation may rescue the absence of OL differentiation because of a loss of total Akt.

We completed a number of molecular and morphologic analyses using several *Akt* KO lines. First, we prepared samples from the cortex and the CC in *Akt1*$^{-/-}$, *Akt2*$^{-/-}$ or *Akt3*$^{-/-}$ mice aged at P14. Western analyses confirmed undetectable bands for Akt1, Akt2 or Akt3 in *Akt1*$^{-/-}$, *Akt2*$^{-/-}$ or *Akt3*$^{-/-}$ mice,
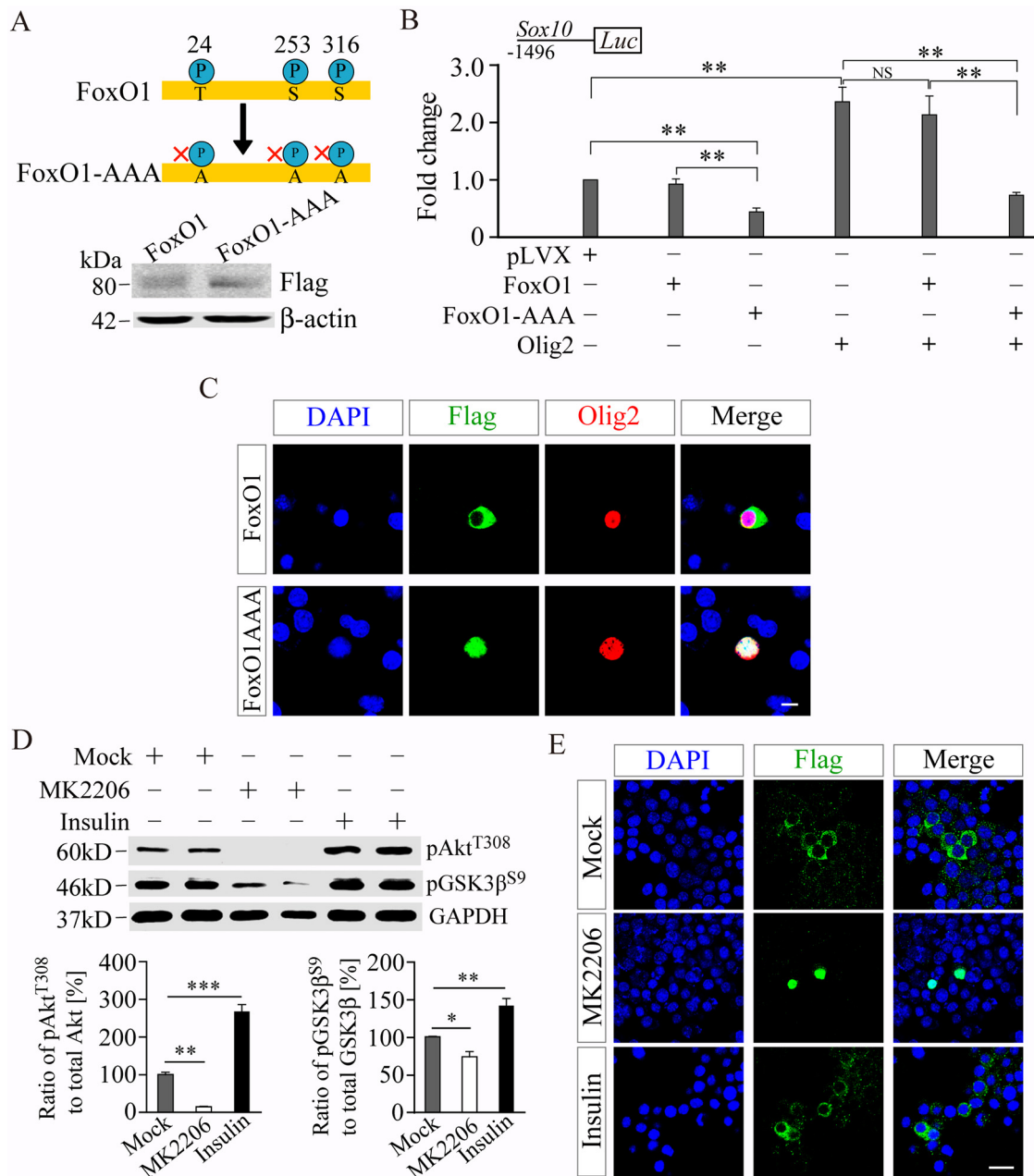
Figure 9. Phosphorylation of FoxO1 by Akt is critical for *Sox10* expression. **A**, Three amino acids, T24, S253, and S316, in WT mouse FoxO1 were mutated to alanines (FoxO1-AAA). FoxO1 and FoxO1-AAA were detected by Western blotting. **B**, Luciferase activity assay. N2a cells were transfected with a vector carrying *Sox10* promoter-driven luciferase reporter together with one expressing pLVX, FoxO1, FoxO1-AAA, Olig2, Olig2/FoxO1, or Olig2/FoxO1-AAA. The *Sox10* promoter was 1496 bp upstream of the TSS. The luciferase activity was measured 24 h after the transfection. Values were averaged from three independent experiments. Data represent the mean ± SEM. There was no significant difference on the luciferase activity between the pLVX and the FoxO1 groups or between the Olig2 and Olig2/FoxO1 groups (NS, not significant). In contrast, there was significant difference in the luciferase activity between the FoxO1 and the FoxO1-AAA groups or between the Olig2/FoxO1 and Olig2/FoxO1-AAA groups. $**p < 0.01$. $n = 3$ independent experiments; one-way ANOVA. **C**, Double immunostaining for Olig2 and Flag. N2a cells were transfected with a plasmid expressing Olig2 together with a vector carrying Flag-FoxO1 or Flag-FoxO1-AAA. Flag-FoxO1 was mainly expressed in the cytoplasm of N2a cells. Flag-FoxO1-AAA and Olig2 were detected in the nucleus. Scale bar, 10 μm. **D**, Western blotting for pAkt^{T308} and pGSK3β^{S9}. N2a cells were transfected with a vector carrying Flag-FoxO1 for 24 h. N2a cells were treated with Mock, MK2206, or insulin. Twenty-four hours after the treatment, cells were collected for lysate preparation. GAPDH served as the loading control. There were significant differences on relative levels of pAkt^{T308} and pGSK3β^{S9} between Mock-, MK2206-, and insulin-treated groups. $*p < 0.05$; $**p < 0.01$; $***p < 0.005$. $n = 3$ independent experiments; one-way ANOVA. **E**, Fluorescence IHC of Flag. N2a cells were transfected with a vector carrying Flag-FoxO1 for 24 h, and the culture medium contained Mock, MK2206, or insulin. Flag-FoxO1 was mainly detected in the nucleus of N2a cells after the MK2206 treatment. Scale bar, 25 μm.

respectively (Fig. 11A,D,G). Second, we found that levels for pFoxO1^{Ser256} and Sox10 were not different between wild-type (WT) and $Akt1^{-/-}$ mice (Fig. 11A). Similar results were obtained for $Akt2^{-/-}$ and $Akt3^{-/-}$ mice (Fig. 11D,G). Third, we conducted IHC analysis on CC1 using brain sections at P14 (Fig. 11B,E,H). There was no significant reduction on the number of

CC1$^+$ cells in the CC in $Akt1^{-/-}$ mice compared with WTs (Fig. 11C). Results for $Akt2^{-/-}$ (Fig. 11F) or $Akt3^{-/-}$ (Fig. 11I) animals were identical. Overall, the above results suggest that pFoxO1 levels are restored by partial preservation of Akt function, and that restoration of FoxO1 phosphorylation may rescue OL differentiation caused by the loss of total Akt.
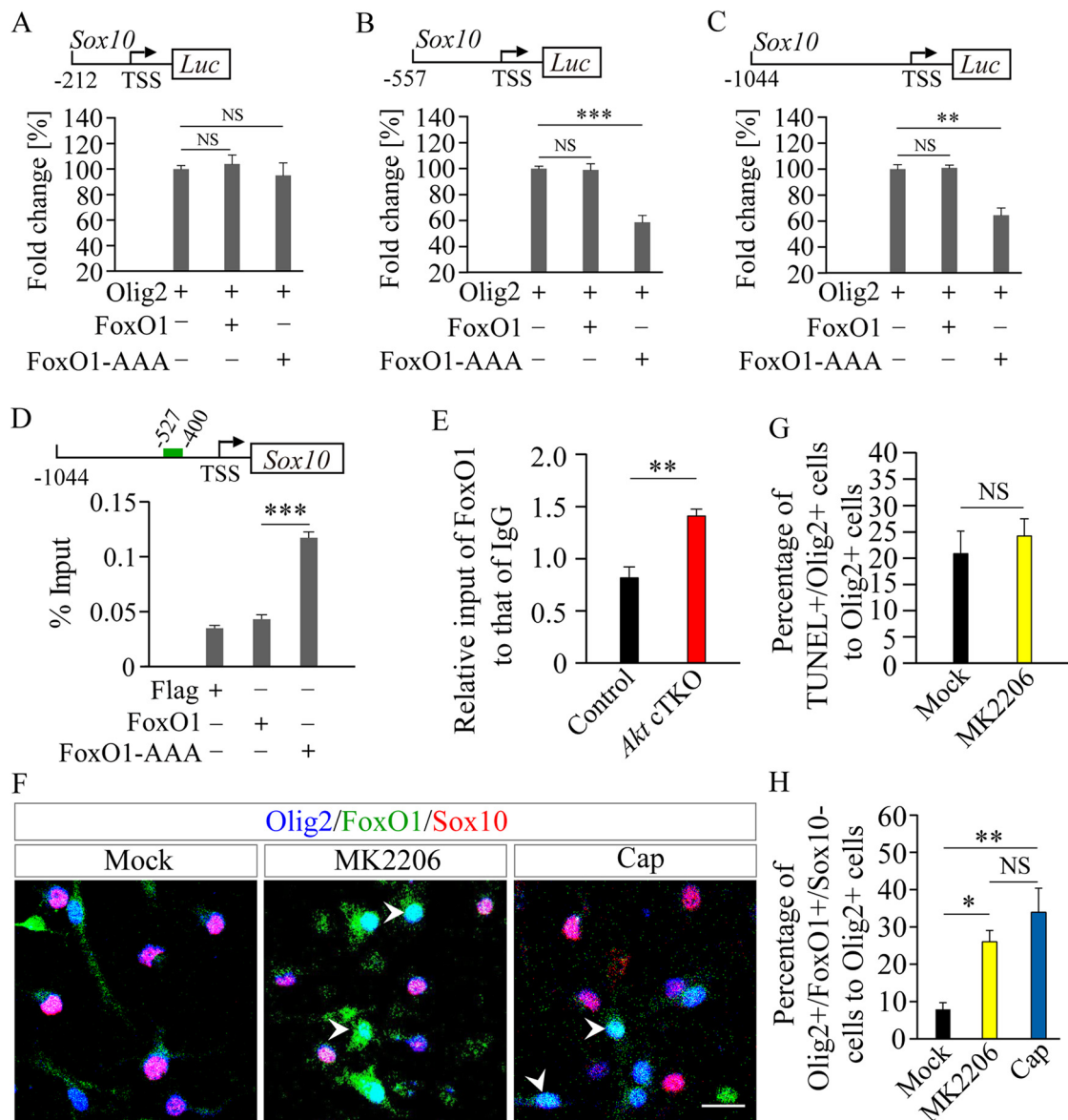
Figure 10. Nonphosphorylated FoxO1 is enriched in the *Sox10* promoter. *A–C*, Various fragments of the *Sox10* promoter were constructed for luciferase assay. Fragment 1, 2, or 3 contained the region of 212 bp (*A*), 557 bp (*B*), or 1044 bp (*C*) upstream of the TSS in the *Sox10* promoter, respectively. The luciferase activity for each fragment was not significantly different between the Olig2/FoxO1 and the Olig2 groups (*A–C*). *A*, The luciferase activity for Fragment1 was not different between the Olig2 and the Olig2/FoxO1-AAA groups. *B*, *C*, The luciferase activity for Fragment2 (*B*) or Fragment3 (*C*) was significantly different between the Olig2 and the Olig2/FoxO1-AAA groups. ✱✱$p < 0.01$; ✱✱✱$p < 0.005$. NS, Not significant. $n = 3$ independent experiments; one-way ANOVA. *D*, ChIP–qRT-PCR analysis using N2a cells. Compared with FoxO1, FoxO1-AAA was enriched in the *Sox10* promoter. The GREEN line illustrates the −527 bp to approximately −400 bp region. N2a cells were transfected with plasmid expressing Flag, FoxO1, or FoxO1-AAA. ✱✱✱$p < 0.005$. $n = 3$ independent experiments; one-way ANOVA. *E*, ChIP–qRT-PCR analysis using mouse tissues. Samples were prepared from the cortex and the CC in control and *Akt* cTKO mice at P7. Input for FoxO1 to that for IgG was defined as relative enrichment of FoxO1 in the *Sox10* promoter. The latter exhibited significant difference between two groups of mice. ✱✱$p < 0.01$. $n = 3$ independent experiments. *F*, Representative images for costaining of Olig2/FoxO1/Sox10 in cultured OPCs. Primary OPC cultures were treated with Mock, MK2206 (0.5 μM), or Cap (0.5 μM) for 1 d. Arrowheads indicated Olig2$^+$ cells, which were negative for Sox10. Scale bar, 20 μm. *G*, Quantification results for TUNEL$^+$/Olig2$^+$ cells in OPC cultures. There was no significant difference on the percentage of TUNEL$^+$/Olig2$^+$ cells to total Olig2$^+$ cells between Mock- and MK2206-treated cultures. $n = 3–4$ independent experiments. *H*, Quantification results for Olig2$^+$/FoxO1$^+$/Sox10$^-$ cells in OPC cultures. There were significant differences in the percentage of Olig2$^+$/FoxO1$^+$/Sox10$^-$ cells to total Olig2$^+$ cells among Mock-, MK2206-, and Cap-treated cultures. ✱$p < 0.05$; ✱✱$p < 0.01$. $n = 3–4$ independent experiments.

Discussion

Akt is implicated in brain disorders associated with WM abnormalities, but the underlying molecular mechanisms are poorly understood (Boland et al., 2007; Ballif et al., 2012; Poduri et al., 2012; Rivière et al., 2012; Thierry et al., 2012; Gai et al., 2015). Although several recent studies have investigated the role of Akt in myelination (Flores et al., 2008; Narayanan et al., 2009; Domènech-Estévez et al., 2016), it remains unknown whether Akt is important for OL differentiation. Since germline deletion of Akt three isoforms leads to early embryonic lethality in mice

(Dummler and Hemmings, 2007; Wang et al., 2015), this has precluded the possibility to use *Akt1/Akt2/Akt3* straight KO mice to investigate *in vivo* function of Akt in the WM. In this study, we took advantage of OL lineage cell-specific *Akt* cTKO mice and obtained the following novel findings. First, the loss of total Akt mediated by *Olig1-Cre* prevents OL differentiation but does not significantly affect neuronal development in the CNS. Second, the loss of total Akt causes downregulation of Sox10. Third, mutant FoxO1 without Akt phosphorylation represses the promoter activity of *Sox10* and is enriched in the *Sox10*

promoter. Overall, phosphorylation of FoxO1 by Akt may be critical for *Sox10* expression and OL differentiation.

Gain-of-function models have recently been used to study the role of Akt in myelination. First, mice expressing a constitutively active Akt (Akt-DD) exhibit enhanced myelination, but the number of OLs in the CNS remains unchanged (Flores et al., 2008; Narayanan et al., 2009). Second, mice expressing an activated form of Akt display thicker myelin sheaths in the peripheral nervous system than controls (Domènech-Estévez et al., 2016). Third, this study used a loss-of-function model to investigate physiological functions of Akt in the WM. We have shown that *Akt* cTKO OPCs are unable to differentiate into mature OLs. Since the deletion of Akt three isoforms does not induce enhanced apoptosis, this excludes the possibility that the complete loss of mature OLs in *Akt* cTKOs may be because of abnormal cell death. In line with the concept that Sox10 is a key TF to control OL differentiation (Kuhlbrodt et al., 1998; Britsch et al., 2001; Stolt et al., 2002; Elbaz and Popko, 2019), the expression of Sox10 is significantly reduced in *Akt* cTKO OPCs at a stage when OLs have not developed. It is reasonable to conclude that the downregulation of Sox10 may serve as the molecular basis for the OL differentiation defect in *Akt* cTKO mice.

Complete myelin loss was observed in *Akt* cTKO mice in this study. This finding is in line with previous studies showing that overexpression of activated Akt enhances myelination (Flores et al., 2008; Narayanan et al., 2009; Domènech-Estévez et al., 2016). We reason that the myelin loss in *Akt* cTKOs may be directly caused by the complete loss of mature OLs. Since Akt-DD transgenic mice exhibit an unchanged number of mature OLs in the CNS (Flores et al., 2008), it is likely that low expression levels of Akt-DD driven by the *Plp* promoter are insufficient to affect OL differentiation.

Sox10 is an important TF to control OL differentiation (Elbaz and Popko, 2019). Recent evidence has shown that *Sox10* expression is regulated by Olig2 through an evolutionary conserved enhancer (Werner et al., 2007; Küspert et al., 2011). Using a luciferase reporter system, we have shown that mutant FoxO1 (FoxO1-AAA) represses the *Sox10* promoter activity and is enriched in a specific domain in the promoter. In contrast, FoxO1 without mutations on Akt phosphorylation sites is mainly localized in the cytoplasm. We report that Akt inhibition causes nuclear distribution of FoxO1 in primary OPC cultures. Together, these findings highlight a critical role of phosphorylation of FoxO1 by Akt in *Sox10* expression and OL differentiation. Moreover, we have observed that the expression of Olig2 enhances the promoter activity of *Sox10*. Previous studies (Werner et al., 2007; Küspert et al., 2011) together with this one further suggest that *Sox10* expression can be regulated by Olig2 through an enhancer- and a promoter-dependent mechanism.
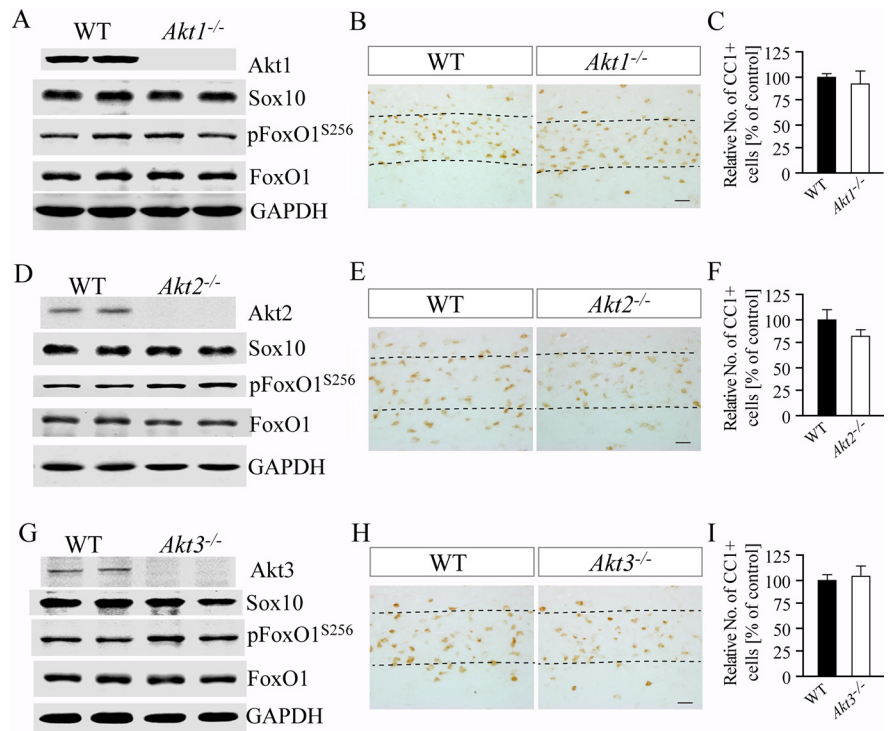

Figure 11. Phosphorylation of FoxO1 and OL populations are unimpaired in Akt single-isoform knock-out mice. *A*, *D*, *G*, Western results on Akt isoforms for Akt single-isoform knock-out mice. Akt1, Akt2, and Akt3 were not detected in *Akt1*$^{-/-}$ (*A*), *Akt2*$^{-/-}$ (*D*), and *Akt3*$^{-/-}$ (*G*) mice at P14, respectively. There were no differences in protein levels of pFoxO1 and Sox10 between WT and Akt single-isoform knock-out mice (*A*, *D*, *G*). GAPDH served as the loading control. *B*, *E*, *H*, Representative IHC images for CC1. The immunoreactivity of CC1 was not different in the CC between WT and Akt single-isoform knock-out mice at P14. Scale bar, 20 μm. *C*, *F*, *I*, Averaged number of CC1$^+$ cells. There was no significant difference in the average number of CC1$^+$ cells in the CC among WT and *Akt1*$^{-/-}$ (*C*), WT and *Akt2*$^{-/-}$ (*F*), or WT and *Akt3*$^{-/-}$ (*I*) at P14.
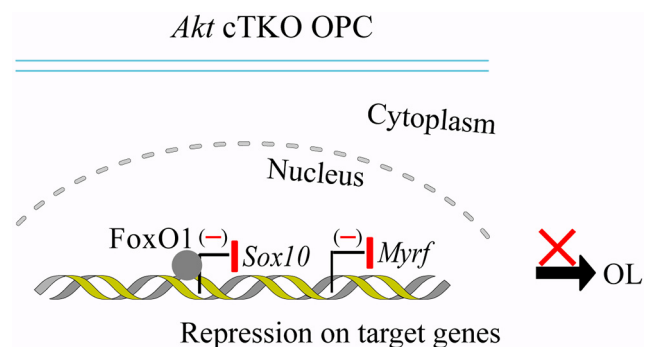

Figure 12. Schematic model for Akt-dependent OL differentiation. This cellular model depicts molecular events involved in Akt-dependent OL differentiation. In *Akt* cTKO OPCs, nonphosphorylated FoxO1 consistently binds to the *Sox10* promoter so that *Sox10* expression is repressed. Reduced Sox10 subsequently inhibits the expression of its downstream genes including *Myrf*, *Mbp*, and *Plp1*. Consequently, OL differentiation is prevented.

Srivastava et al. (2018) have recently shown that WM injury (WMI) triggers the accumulation of bioactive hyaluronan fragment (bHAf) to induce deficit in myelination. They found that bHAf selectively blocks OL differentiation in a maturation-dependent fashion via the noncanonical TLR4/TRIF pathway, which inactivates Akt and promotes persistent activation of FoxO3 (Srivastava et al., 2018). They reported that the overexpression of FoxO3 downregulates Mbp expression through interactions with Brg1 and Olig2 in promoters of *FoxO3* and *Mbp* (Srivastava et al., 2018). Unlike the WMI model used in the

above study, the *Akt* cTKO mouse was used here to investigate *in vivo* function of Akt in OL development. We found that FoxO1 levels were not significantly changed in *Akt* cTKO mice, and that phosphorylation of FoxO1 was blocked in *Akt* cTKO OPCs. Srivastava et al. (2018) have shown that activated FoxO3 may interact with Brg1 and Olig2 to regulate Mbp expression. Here, we demonstrated that nonphosphorylated FoxO1 may bind to the *Sox10* promoter to repress *Sox10* expression, which subsequently inhibits Mbp expression. Overall, the work by Srivastava et al. (2018) suggests that Akt is involved in bHAf-dependent OL differentiation after the WMI takes place. The present study reveals that physiological functions of Akt in OPCs are to regulate Sox10 expression and promote OL differentiation in the CNS.

To summarize the above findings, we propose a working model as follows. In *Akt* cTKO OPCs, FoxO1 cannot be phosphorylated at Akt-targeted sites because of the inactivation of all Akt isoforms. Nonphosphorylated FoxO1 consistently binds to the *Sox10* promoter to repress *Sox10* expression (Fig. 12). Subsequently, the downregulation of Sox10 inhibits the expression of *Myrf* and downstream myelin genes including *Mbp* and *Plp1*. As a consequence, OL differentiation cannot be triggered in *Akt* cTKO OPCs (Fig. 12). In contrast, Akt phosphorylates FoxO1 to promote its cytoplasmic translocation so that *Sox10* expression is activated in control OPCs. Sox10 then induces the expression of *Myrf* and myelin genes, which promotes OL differentiation (Fig. 12). Together, this study identifies a novel phosphorylation-dependent mechanism to regulate Sox10 expression and OL differentiation.

References

Ballif BC, Rosenfeld JA, Traylor R, Theisen A, Bader PI, Ladda RL, Sell SL, Steinraths M, Surti U, McGuire M, Williams S, Farrell SA, Filiano J, Schnur RE, Coffey LB, Tervo RC, Stroud T, Marble M, Netzloff M, Hanson K, et al. (2012) High-resolution array CGH defines critical regions and candidate genes for microcephaly, abnormalities of the corpus callosum, and seizure phenotypes in patients with microdeletions of 1q43q44. Hum Genet 131:145–156.

Boland E, Clayton-Smith J, Woo VG, McKee S, Manson FDC, Medne L, Zackai E, Swanson EA, Fitzpatrick D, Millen KJ, Sherr EH, Dobyns WB, Black GCM (2007) Mapping of deletion and translocation breakpoints in 1q44 implicates the serine/threonine kinase AKT3 in postnatal microcephaly and agenesis of the corpus callosum. Am J Hum Genet 81:292–303.

Britsch S, Goerich DE, Riethmacher D, Peirano RI, Rossner M, Nave KA, Birchmeier C, Wegner M (2001) The transcription factor Sox10 is a key regulator of peripheral glial development. Genes Dev 15:66–78.

Brunet A, Bonni A, Zigmond MJ, Lin MZ, Juo P, Hu LS, Anderson MJ, Arden KC, Blenis J, Greenberg ME (1999) Akt promotes cell survival by phosphorylating and inhibiting a Forkhead transcription factor. Cell 96:857–868.

Cai J, Chen Y, Cai WH, Hurlock EC, Wu H, Kernie SG, Parada LF, Lu QR (2007) A crucial role for Olig2 in white matter astrocyte development. Development 134:1887–1899.

Cheng S, Liu T, Hu Y, Xia Y, Hou J, Huang C, Zou X, Liang J, Stone Shi Y, Zheng Y, Lu J, Chen G (2019) Conditional inactivation of Pen-2 in the developing neocortex leads to rapid switch of apical progenitors to basal progenitors. J Neurosci 39:2195–2207.

Domènech-Estévez E, Baloui H, Meng XS, Zhang YQ, Deinhardt K, Dupree JL, Einheber S, Chrast R, Salzer JL (2016) Akt regulates axon wrapping and myelin sheath thickness in the PNS. J Neurosci 36:4506–4521.

Dummler B, Hemmings BA (2007) Physiological roles of PKB/Akt isoforms in development and disease. Biochem Soc Trans 35:231–235.

Easton RM, Cho H, Roovers K, Shineman DW, Mizrahi M, Forman MS, Lee VM, Szabolcs M, de Jong R, Oltersdorf T, Ludwig T, Efstratiadis A, Birnbaum MJ (2005) Role for Akt3/protein kinase B gamma in attainment of normal brain size. Mol Cell Biol 25:1869–1878.

Elbaz B, Popko B (2019) Molecular control of oligodendrocyte development. Trends Neurosci 42:263–277.

Emery B, Agalliu D, Cahoy JD, Watkins TA, Dugas JC, Mulinyawe SB, Ibrahim A, Ligon KL, Rowitch DH, Barres BA (2009) Myelin gene regulatory factor is a critical transcriptional regulator required for CNS myelination. Cell 138:172–185.

Flores AI, Narayanan SP, Morse EN, Shick HE, Yin X, Kidd G, Avila RL, Kirschner DA, Macklin WB (2008) Constitutively active Akt induces enhanced myelination in the CNS. J Neurosci 28:7174–7183.

Fruman DA, Chiu H, Hopkins BD, Bagrodia S, Cantley LC, Abraham RT (2017) The PI3K pathway in human disease. Cell 170:605–635.

Gai D, Haan E, Scholar M, Nicholl J, Yu S (2015) Phenotypes of AKT3 deletion: a case report and literature review. Am J Med Genet A 167A:174–179.

He DY, Marie C, Zhao CT, Kim B, Wang JC, Deng YQ, Clavairoly A, Frah M, Wang HB, He XL, Hmidan H, Jones BV, Witte D, Zalc B, Zhou X, Choo DI, Martin DM, Parras C, Lu QR (2016) Chd7 cooperates with Sox10 and regulates the onset of CNS myelination and remyelination. Nat Neurosci 19:678–689.

Hirai H, Sootome H, Nakatsuru Y, Miyama K, Taguchi S, Tsujioka K, Ueno Y, Hatch H, Majumder PK, Pan BS, Kotani H (2010) MK-2206, an allosteric Akt inhibitor, enhances antitumor efficacy by standard chemotherapeutic agents or molecular targeted drugs in vitro and in vivo. Mol Cancer Ther 9:1956–1967.

Hou J, Bi H, Ye Z, Huang W, Zou G, Zou X, Shi Y, Shen Y, Ma Q, Kirchhoff F, Hu Y, Chen G (2021) Pen-2 negatively regulates the differentiation of oligodendrocyte precursor cells into astrocytes in the central nervous system. J Neurosci 41:4976–4990.

Huang C, Liu T, Wang Q, Hou W, Zhou C, Song Z, Shi Y, Gao X, Chen G, Yin Z, Hu Y (2020) Loss of PP2A disrupts the retention of radial glial progenitors in the telencephalic niche to impair the generation for late-born neurons during cortical development. Cereb Cortex 30:4183–4196.

Kuhlbrodt K, Herbarth B, Sock E, Hermans-Borgmeyer I, Wegner M (1998) Sox10, a novel transcriptional modulator in glial cells. J Neurosci 18:237–250.

Küspert M, Hammer A, Michael RB, Wegner M (2011) Olig2 regulates Sox10 expression in oligodendrocyte precursors through an evolutionary conserved distal enhancer. Nucleic Acids Res 39:1280–1293.

Levenga J, Wong H, Milstead RA, Keller BN, LaPlante L, Hoeffer CA (2017) AKT isoforms have distinct hippocampal expression and roles in synaptic plasticity. Elife 6:e30640.

Lu QR, Sun T, Zhu ZM, Ma N, Garcia M, Stiles CD, Rowitch DH (2002) Common developmental requirement for Olig function indicates a motor neuron/oligodendrocyte connection. Cell 109:75–86.

Manning BD, Cantley LC (2007) AKT/PKB signaling: navigating downstream. Cell 129:1261–1274.

Manning BD, Toker A (2017) AKT/PKB signaling: navigating the network. Cell 169:381–405.

Matsuzaki H, Daitoku H, Hatta M, Aoyama H, Yoshimochi K, Fukamizu A (2005) Acetylation of Foxo1 alters its DNA-binding ability and sensitivity to phosphorylation. Proc Natl Acad Sci U S A 102:11278–11283.

Mayoral SR, Chan JR (2016) The environment rules: spatiotemporal regulation of oligodendrocyte differentiation. Curr Opin Neurobiol 39:47–52.

Muzumdar MD, Tasic B, Miyamichi K, Li L, Luo L (2007) A global double-fluorescent Cre reporter mouse. Genesis 45:593–605.

Nakae J, Park BC, Accili D (1999) Insulin stimulates phosphorylation of the forkhead transcription factor FKHR on serine 253 through wortmannin-sensitive pathway. J Biol Chem 274:15982–15985.

Narayanan SP, Flores AI, Wang F, Macklin WB (2009) Akt signals through the mammalian target of rapamycin pathway to regulate CNS myelination. J Neurosci 29:6860–6870.

Nishiyama C, Uesaka T, Manabe T, Yonekura Y, Nagasawa T, Newgreen DF, Young HM, Enomoto H (2012) Trans-mesenteric neural crest cells are the principal source of the colonic enteric nervous system. Nat Neurosci 15:1211–1218.

Niu JQ, Wang LY, Liu SB, Li CR, Kong JM, Shen HY, Xiao L (2012a) An efficient and economical culture approach for the enrichment of purified oligodendrocyte progenitor cells. J Neurosci Methods 209:241–249.

Niu JQ, Mei F, Wang LY, Liu SB, Tian YP, Mo W, Li HL, Lu QR, Xiao L (2012b) Phosphorylated olig1 localizes to the cytosol of oligodendrocytes and promotes membrane expansion and maturation. Glia 60:1427–1436.

Pearce LR, Komander D, Alessi DR (2010) The nuts and bolts of AGC protein kinases. Nat Rev Mol Cell Biol 11:9–22.

Poduri A, Evrony GD, Cai X, Elhosary PC, Beroukhim R, Lehtinen MK, Hills LB, Heinzen EL, Hill A, Hill RS, Barry BJ, Bourgeois BFD, Riviello JJ, Barkovich AJ, Black PM, Ligon KL, Walsh CA (2012) Somatic activation of AKT3 causes hemispheric developmental brain malformations. Neuron 74:41–48.

Rivière J-B, Mirzaa GM, O'Roak BJ, Beddaoui M, Alcantara D, Conway RL, St-Onge J, Schwartzentruber JA, Gripp KW, Nikkel SM, Worthylake T, Sullivan CT, Ward TR, Butler HE, Kramer NA, Albrecht B, Armour CM, Armstrong L, Caluseriu O, Cytrynbaum C, et al. (2012) De novo germline and postzygotic mutations in AKT3, PIK3R2 and PIK3CA cause a spectrum of related megalencephaly syndromes. Nat Genet 44:934–940.

Rowitch DH, Kriegstein AR (2010) Developmental genetics of vertebrate glial-cell specification. Nature 468:214–222.

Schäffner I, Minakaki G, Khan MA, Balta EA, Schlötzer-Schrehardt U, Schwarz TJ, Beckervordersandforth R, Winner B, Webb AE, DePinho RA, Paik J, Wurst W, Klucken J, Lie DC (2018) FoxO function is essential for maintenance of autophagic flux and neuronal morphogenesis in adult neurogenesis. Neuron 99:1188–1203.

Setoguchi T, Kondo T (2004) Nuclear export of OLIG2 in neural stem cells is essential for ciliary neurotrophic factor-induced astrocyte differentiation. J Cell Biol 166:963–968.

Shapiro LA, Wang L, Ribak CE (2008) Rapid astrocyte and microglial activation following pilocarpine-induced seizures in rats. Epilepsia 49 [Suppl 2]:33–41.

Silbereis JC, Nobuta H, Tsai H-H, Heine VM, McKinsey GL, Meijer DH, Howard MA, Petryniak MA, Potter GB, Alberta JA, Baraban SC, Stiles CD, Rubenstein JLR, Rowitch DH (2014) Olig1 function is required to repress Dlx1/2 and interneuron production in mammalian brain. Neuron 81:574–587.

Srivastava T, Diba P, Dean JM, Banine F, Shaver D, Hagen M, Gong X, Su WP, Emery B, Marks DL, Harris EN, Baggenstoss B, Weigel PH, Sherman LS, Back SA (2018) A TLR/AKT/FoxO3 immune tolerance-like pathway disrupts the repair capacity of oligodendrocyte progenitors. J Clin Invest 128:2025–2041.

Stolt CC, Rehberg S, Ader M, Lommes P, Riethmacher D, Schachner M, Bartsch U, Wegner M (2002) Terminal differentiation of myelin-forming oligodendrocytes depends on the transcription factor Sox10. Genes Dev 16:165–170.

Sun SH, Zhu XJ, Huang H, Guo W, Tang T, Xie BH, Xu XF, Zhang ZY, Shen Y, Dai ZM, Qiu M (2019) WNT signaling represses astrogliogenesis via Ngn2-dependent direct suppression of astrocyte gene expression. Glia 67:1333–1343.

Thierry G, Bénéteau C, Pichon O, Flori E, Isidor B, Popelard F, Delrue M-A, Duboscq-Bidot L, Thuresson A-C, van Bon BWM, Cailley D, Rooryck C, Paubel A, Metay C, Dusser A, Pasquier L, Béri M, Bonnet C, Jaillard S, Dubourg C, et al. (2012) Molecular characterization of 1q44 microdeletion in 11 patients reveals three candidate genes for intellectual disability and seizures. Am J Med Genet A 158A:1633–1640.

Tremblay RG, Sikorska M, Sandhu JK, Lanthier P, Ribecco-Lutkiewicz M, Bani-Yaghoub M (2010) Differentiation of mouse Neuro 2A cells into dopamine neurons. J Neurosci Methods 186:60–67.

Tschopp O, Yang ZZ, Brodbeck D, Dummler BA, Hemmings-Mieszczak M, Watanabe T, Michaelis T, Frahm J, Hemmings BA (2005) Essential role of protein kinase B gamma (PKB gamma/Akt3) in postnatal brain development but not in glucose homeostasis. Development 132:2943–2954.

van der Vos KE, Coffer PJ (2008) FOXO-binding partners: it takes two to tango. Oncogene 27:2289–2299.

Wang H, Zhang B, Zhang T, Wang L, Zou X, Xu Y, Chen L, Chen G (2017) Impaired spatial learning is associated with disrupted integrity of the white matter in Akt3 knockout mice. CNS Neurosci Ther 23:99–102.

Wang H, Liu M, Zou G, Wang L, Duan W, He X, Ji M, Zou X, Hu Y, Yang J, Chen G (2021) Deletion of PDK1 in oligodendrocyte lineage cells causes white matter abnormality and myelination defect in the central nervous system. Neurobiol Dis 148:105212.

Wang L, Cheng S, Yin Z, Xu C, Lu S, Hou J, Yu T, Zhu X, Zou X, Peng Y, Xu Y, Yang Z, Chen G (2015) Conditional inactivation of Akt three isoforms causes tau hyperphosphorylation in the brain. Mol Neurodegener 10:33.

Weng Q, Chen Y, Wang H, Xu X, Yang B, He Q, Shou W, Chen Y, Higashi Y, van den Berghe V, Seuntjens E, Kernie SG, Bukshpun P, Sherr EH, Huylebroeck D, Lu QR (2012) Dual-mode modulation of Smad signaling by Smad-interacting protein Sip1 is required for myelination in the central nervous system. Neuron 73:713–728.

Werner T, Hammer A, Wahlbuhl M, Bosl MR, Wegner M (2007) Multiple conserved regulatory elements with overlapping functions determine Sox10 expression in mouse embryogenesis. Nucleic Acids Res 35:6526–6538.

Xu C, Yu L, Hou J, Jackson J, Wang H, Huang C, Liu T, Wang Q, Zou X, Morris R, Spires-Jones T, Y Z, Yin Z, Xu Y, Chen G (2017) Conditional deletion of PDK1 in the forebrain causes neuron loss and increased apoptosis during cortical development. Front Cell Neurosci 11:330.

Yamagata K, Daitoku H, Takahashi Y, Namiki K, Hisatake K, Kako K, Mukai H, Kasuya Y, Fukamizu A (2008) Arginine methylation of FOXO transcription factors inhibits their phosphorylation by Akt. Mol Cell 32:221–231.

Yang F, Wang JC, Han JL, Zhao G, Jiang W (2008) Different effects of mild and severe seizures on hippocampal neurogenesis in adult rats. Hippocampus 18:460–468.

Zhang LG, He XL, Liu L, Jiang MQ, Zhao CT, Wang HB, He DY, Zheng T, Zhou XY, Hassan A, Ma ZX, Xin M, Sun Z, Lazar MA, Goldman SA, Olson EN, Lu QR (2016) Hdac3 interaction with p300 histone acetyltransferase regulates the oligodendrocyte and astrocyte lineage fate switch. Dev Cell 36:316–330.

Zhang T, Shi Z, Wang Y, Wang L, Zhang B, Chen G, Wan Q, Chen L (2019) Akt3 deletion in mice impairs spatial cognition and hippocampal CA1 long long-term potentiation through downregulation of mTOR. Acta Physiol (Oxf) 225:e13167.

Zhao Y, Yang J, Liao W, Liu X, Zhang H, Wang S, Wang D, Feng J, Yu L, Zhu WG (2010) Cytosolic FoxO1 is essential for the induction of autophagy and tumour suppressor activity. Nat Cell Biol 12:665–675.

Zhu Q, Zhao XF, Zheng K, Li H, Huang H, Zhang ZY, Mastracci T, Wegner M, Chen YP, Sussel L, Qiu MS (2014) Genetic evidence that Nkx2.2 and Pdgfra are major determinants of the timing of oligodendrocyte differentiation in the developing CNS. Development 141:548–555.

Zhu XQ, Bergles DE, Nishiyama A (2008) NG2 cells generate both oligodendrocytes and gray matter astrocytes. Development 135:145–157.